DIGITAL OUTCROP MODELING OF HOFUF OUTCROP VIA INTEGRATING LIDAR, GROUND PENETRATING RADAR AND SEDIMENTOLOGY, EASTERN PROVINCE SAUDI ARABIA

BY

Mohammed Yousef Abdullah

A Thesis Presented to the
DEANSHIP OF GRADUATE STUDIES

KING FAHD UNIVERSITY OF PETROLEUM & MINERALS

DHAHRAN, SAUDI ARABIA

In Partial Fulfillment of the
Requirements for the Degree of

MASTER OF SCIENCE

In

GEOPHYSICS

May, 2013

KING FAHD UNIVERSITY OF PETROLEUM & MINERALS

DHAHRAN- 31261, SAUDI ARABIA

DEANSHIP OF GRADUATE STUDIES

This thesis, written by **Mohammed Yousef Abdullah** under the direction his thesis advisor and approved by his thesis committee, has been presented and accepted by the Dean of Graduate Studies, in partial fulfillment of the requirements for the degree of **MASTER OF SCIENCE IN GEOPHYSICS.**

Dr. Gabor Korvin
(Advisor)

Dr. Abdulaziz Al-Shaibani
Department Chairman

Dr. Osman Abdulatif
(Member)

Dr. Salam A. Zummo
Dean of Graduate Studies

Dr. Abdulwahab Abo Khodair
(Member)

28/5/13
Date

Dedication

To my lovely parents

ACKNOWLEDGMENTS

I want to acknowledge my big brother Dr. Hassan Eltom for his help and suggestions in the sedimentology and LIDAR parts. Also, I thank Dr. Abdullatif A. Al-Shuhail for his help in ground penetrating radar processing. Also, I want to thank my brothers and colleagues who helped me in field and lab work in sedimentology part. Finally, a lot of thanks to my committee for reviewing my thesis especially my advisor Dr. Gabor Korvin.

TABLE OF CONTENTS

LIST OF TABLES

LIST OF FIGURES

ABSTRACT

Full Name : Mohammed Yousef Hussein Abdullah

Thesis Title : Digital Outcrop Modeling of Hofuf Outcrop via integrating LIDAR, Ground Penetrating Radar and Sedimentology, Eastern Province, Saudi Arabia

Major Field : Geophysics

Date of Degree : May 2013

Late Miocene-Early Pliocene Hofufoutcrop is located in the eastern province. The aims of this study are to determine the depositional environment, to build surface outcrop models(facies and porosity models) using sedimentology, image the subsurface through the Ground Penetrating Radar to detect the reflectors and image the face of the outcrop via terrestrial laser scanning (LIDAR) and integrate it with ground penetrating radar data to track these layers detected by the radar on LIDAR's image.

ملخص الرسالة

الاسم الكامل:محمد يوسف حسين عبدالله

عنوان الرسالة:النمذجة الرقمية لمنكشف الهفوف عبر دمج الليدار، الرادار الأرضي وعلم الرسوبيات في المنطقة الشرقية من المملكة العربية السعودية

التخصص: جيوفيزياء

تاريخ الدرجة العلمية:مايو 2013

منكشف الهفوف يقع في المنطقة الشرقية من المملكة العربية السعودية. العمر الجيولوجي المقدر لمنكشف الهفوف هو ما بين أواخر المايوسين وبدايات البلايوسين. تهدف الدراسة إلى بناء نماذج للمنكشف تظهر توزيع السحنات وكذلك المسامية عن طريق دراسة العينات المجموعة من المنكشف. بالنسبة للرادار الأرضي سيستخدم للكشف عن العواكس التي تمثل الحدود بين السحنات والتي تظهر بسبب اختلاف السماحية الكهربية. جهاز الليدار يقوم بتصوير السطح الجانبي للمنكشف ومن ثم نقوم بتتبع العواكس التي كشفها الرادر الأرضي والتي تكون ظاهرة على صورة الليدار.

CHAPTER 1

INTRODUCTION

Outcrop models play an important role in studying analogues and understanding some parameters that could not be easy to accomplish from the subsurface data of equivalent fields like facies distribution or size of grains of the sediments, geometry and architecture of an equivalent reservoir. These acquired outcrop data have wide range of scales (km to mm) and can fill the gap between seismic and well data of the same subsurface reservoirs (Van Lanen et al., 2009). There are several methods used to collect outcrop data in order to build digital models like Real Time Kinematic (RTK), Airborne Scanning LIDAR, Terrestrial Laser Scanning, Differential GPS, near surface high resolution geophysics like ground penetrating radar, Boreholes (Van Lanen et al., 2009). Table 1 shows these methods and others with their advantages and disadvantages. Although seismic method is not a preferable geophysical method in outcrop studies because of the limitation in its vertical resolution, we can generate a forward seismic model form outcrop data. Forward seismic has many advantages like (Falivene et al., 2010;Tomasso et al., 2010) :

1) Links the information from outcrop with the available information from subsurface.

2) Helps in seismic interpretation for real seismic data because these forward models arederived from well-known geological models.

3) Give clear idea on which geological features can be resolved and identified and which cannot be resolved.

Here in the study Terrestrial Laser Scanning (LIDAR) and Ground Penetrating Radar (GPR) are integrated to study the Hofuf outcrop and for building outcrop analogue models for that outcrop.

Table 1: Outcrop Analogue Digital Data Collection Methods (Pringle et al., 2006)

Digital data collection method	Typical accuracy	Typical application	Advantages	Disadvantages	Typical Cost
Aerial digital photogrammetry	~5-25m	Mapping large-scale stratigraphy & generate digital model framework	Fast, usually third-party acquisition (minutes); large areas covered & fast remote mapping (days)	Slow time processing (days); relatively low resolution & poor on near-vertical outcrop faces	High if survey has to be commissioned. Cheap if existing photos are used
Ground-based digital photogrammetry	~0.1-0.5m	Detailed study of complex outcrop faces	Fast acquisition (minutes); less detailed fieldwork needed	Medium time processing (days) & interpretation	Relatively cheap £600
Calibrated photo logs	~0.2m	Rapid collection of facies thickness and relative surface positions from cliff sections	Fast acquisition (minutes), Fast processing (hours) & rapid model creation	Can suffer from photograph distortion, no high resolution logging	Very cheap £300
Hand-held GPS	~1-5m	Sample point location & regional mapping	Instant locational fix	Significant 'Z' positional error (up to 30m)	Very cheap £150
RTK dGPS	Better than 10mm	Attribute collection, surveying outcrops & accurate base stations	Instant point collection allows 'walking out' of key surfaces, medium time processing (typically a day)	Not possible on near-vertical cliff-faces	Expensive £20ks+
Reflectorless Total Station	3mm at 200m range	Attribute collection, surveying outcrops, good for vertical faces	Instant point collection, data capture on near-vertical cliff faces	Slow to acquire, dGPS data needed to convert to UTM co-ordinates	Moderately expensive £2k
Ground-based LIDAR (laser scanner)	5mm at 200m range	Very rapid collection of outcrop surface topography	Relatively rapid acquisition (minutes);	Significant post processing (days)	Expensive £100k
Bore-hole data	1mm (from core)	Drilled behind outcrop to extend horizons into 3D	Very high resolution data, comparable to outcrop information & reservoir logs	Very slow acquisition (weeks), processing and interpretation (weeks)	Very Expensive £200k +
Near-surface geophysics (GPR in this case)	~0.1-0.5m	Acquired behind outcrop to extend correlated horizons into 3D	Allows 3D information behind outcrop to be acquired	Slow acquisition (days) and processing (days), only works in specific site conditions	Moderately expensive £30k

1.1 Literature Review

1.1.1 Terrestrial Laser Scanning (LIDAR)

Terrestrial Laser Scanning or LIDAR is one of the recent methods in acquiring outcrop data. The concept of LIDAR is that a laser pulse is emitted toward the target, hits the target and get reflected directly to the device (Bellian et al., 2005) Figure 1.

LIDAR usage grew quickly in the last years because of the many favorable features of the device. Some of these features are (Pringle et al., 2006; Bellian et al., 2005):

1) The high resolution of the device that ranges from several meters to a few millimeters.

2) Can reach and image inaccessible areas of the outcrop.

3) In addition to the resolution the device has high precision.

4) Can make several surveys from different angles and sides. Then, merges the images into one full 3D image of the target.

There are some disadvantages of LIDAR, one of them is that because of the high resolution of the data its size is large and it needs sometimes several days in processing.

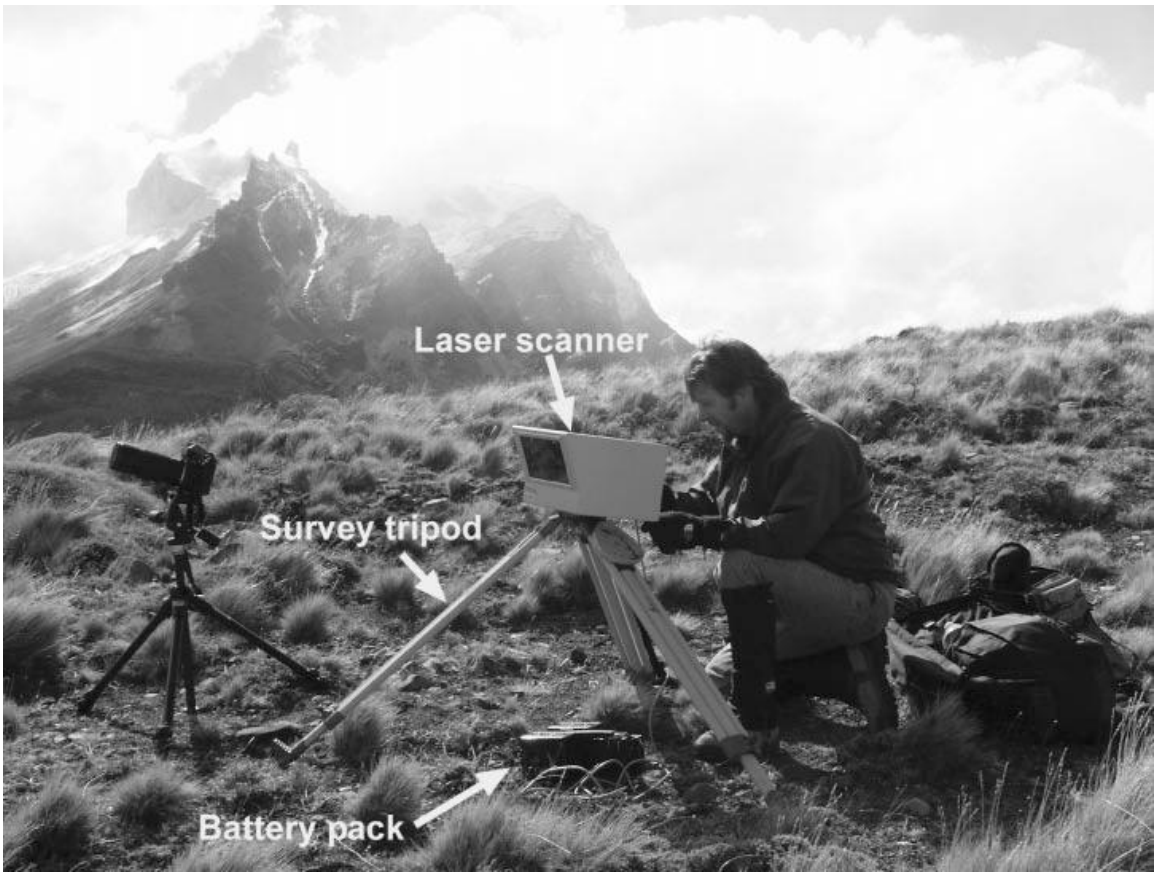

Figure 1: Laser Scanner LIDAR in the field (Bellian et al., 2005).

1.1.2 Ground Penetrating Radar

Ground penetrating radar known shortly as GPR is one of geophysical exploration methods for near surface exploration. GPR theory follows the electromagnetic concept and it has a big similarity with seismic method. Due to that there are some parameters of GPR share the same concept of seismic parameters. For example, the reflection coefficient in seismic exploration (RC) is computed through the following formula:

$$\mathrm{RC} = \frac{Z_2 - Z_1}{Z_2 + Z_1} \tag{1}$$

where:

Z_1 : Acoustic Impedance of the 1st layer

Z_2 : Acoustic Impedance of the 2nd layer

The GPR has also a reflection coefficient computed as:

$$\mathrm{RC} = \frac{\sqrt{K_2} - \sqrt{K_1}}{\sqrt{K_2} + \sqrt{K_1}} \tag{2}$$

where :

K_2 : Dielectric constant of the 2nd layer

K_1 : Dielectric Constant of the 1st layer

Another kind of similarity between GPR and seismic is they have similar processing steps like gain, deconvolution and migration. However, GPR has higher resolution than seismic. So, in terms of near surface investigation GPR provides better images and details

than seismic can provide. Because of that GPR is the preferable geophysical method in outcrop studies (Pringle et al. , 2006). Several studies on outcrops include GPR as a tool to integrate it with other methods like LIDAR (Lee et al. , 2007), or only with sedimentology (McMechan et al. , 1997; Van Dam et al. , 2000; Jorry et al. , 2011). For most sediments the magnetic permeability is near unity (Van Dam et al. , 2000) because of that the electromagnetic wavevelocity (V) can be computed by the following formula:

$$V = \frac{c}{\sqrt{K}} \quad (3)$$

Where:

c : is the speed of light (0.30 m/ns)

K : is the dielectric constant

1.2 Geology of the Area

The paleofcies map of the Miocene age of the formations in Arabian Peninsula Figure 2(Zeigler, 2001) shows the faciesandpaleoenvironments associated with the deposition of the Hadrukh, Dam, and Hofuf formations and their regional equivalents. The paleofacies changes laterally from east to west from shallow marine carbonate / clastic to continental and lacustrine deposits. The Miocene-Pliocene age sedimentary succession in the area consists of both clastic and carbonate rocks. The rock succession is divided into three formations which are from bottom to top are Hadrukh, Dam, Hofuf Formations. The succession is overlain by Quaternary sand, silt and gravel of the Kharj Formation (Powers et al., 1966) Figure 3.In the area of study near the cement factory in Shedgum two formations are noted Dam and Hofuf Formations.

1.2.1 Dam Formation

The Dam formation is named for Jabal al Lidam. The base of the Dam formation changes from the sandstone of the Hadrukh Formation below to fossiliferous marl above. The top is at the contact between marls and limestone with marine fossils of the Dam and overlying clay and sandstone and gravel of the basal Hofuf Formation (Powers et al., 1966). The thickness of the Dam Formation varies in different areas. About 90 m is exposed at the type locality but sometimes reach 30 m or a maximum of 100 m for the full section (Powers et al., 1966). For our case study Hofuf Formation is only exposed in the outcrop.

1.2.2 HOFUF Formation

The Hofuf Formation covers large areas to the west of the Al Hasa Oases; along the coast there are only scattered outcrops from about the latitude of the Al-Hafuf (lat 25 22’ N) to the Qatar Peninsula and beyond. At the type locality the thickness of the Hofuf Formation is about 95 m and consists from base to top of interbedded conglomerate and alternating red and light grey argillaceous limestone. Most of the Hofuf Formation outcrops occupy the crestal zone of the Ghawar Anticline (Saner et al., 2005). The Hofuf Formation represents continental facies and it is estimated to be Miocene to Paleocene (Powers et al., 1966). However, sometimes it is estimated Middle to late Miocene. Figure 4 shows the stratigraphic column for the Dam Formation and Hofuf Formation in Ghawar area (Saner et al., 2005).

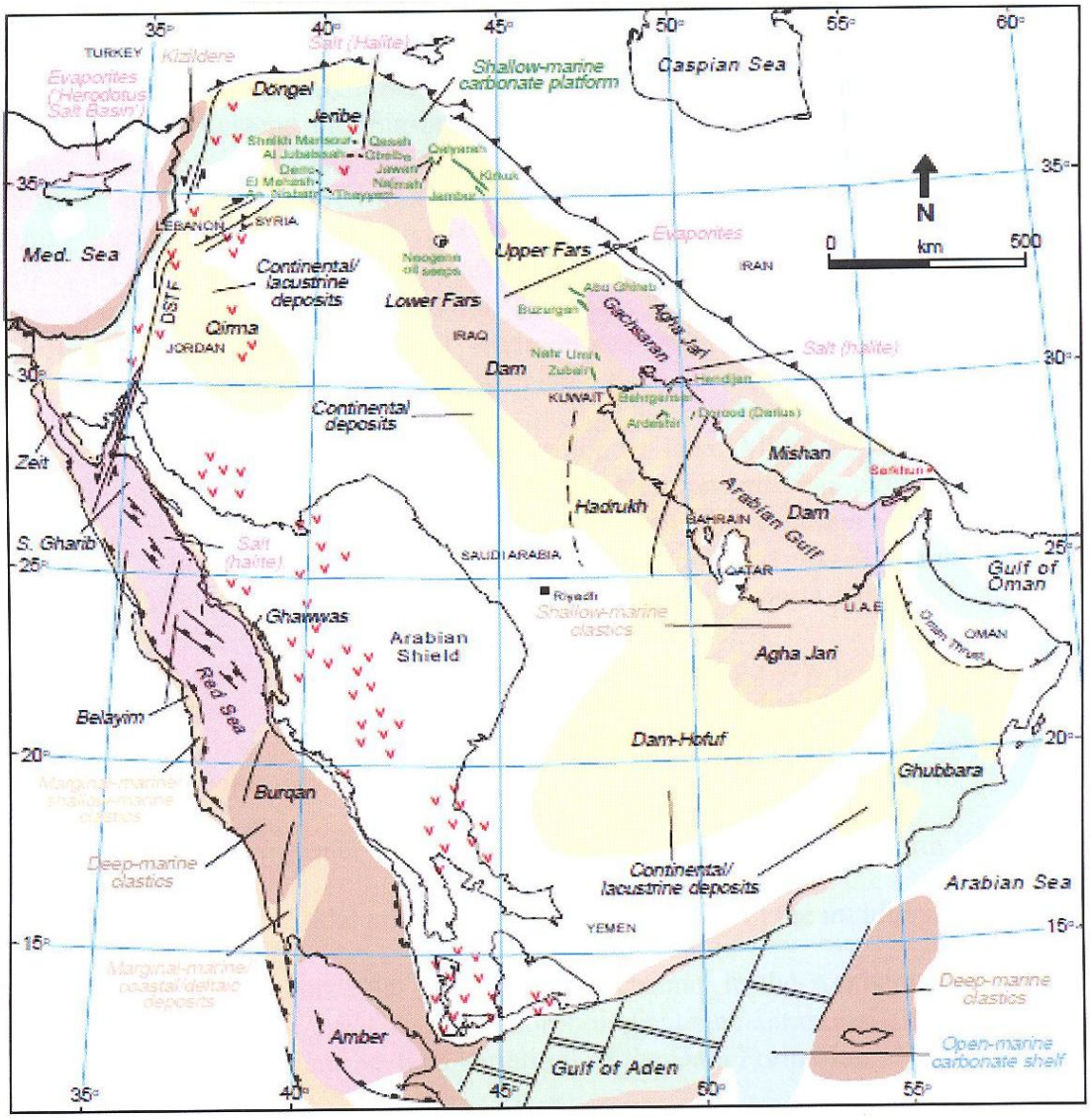

Figure 2: Paleofacies map of Arabian Peninsula (Zeigler, 2001)

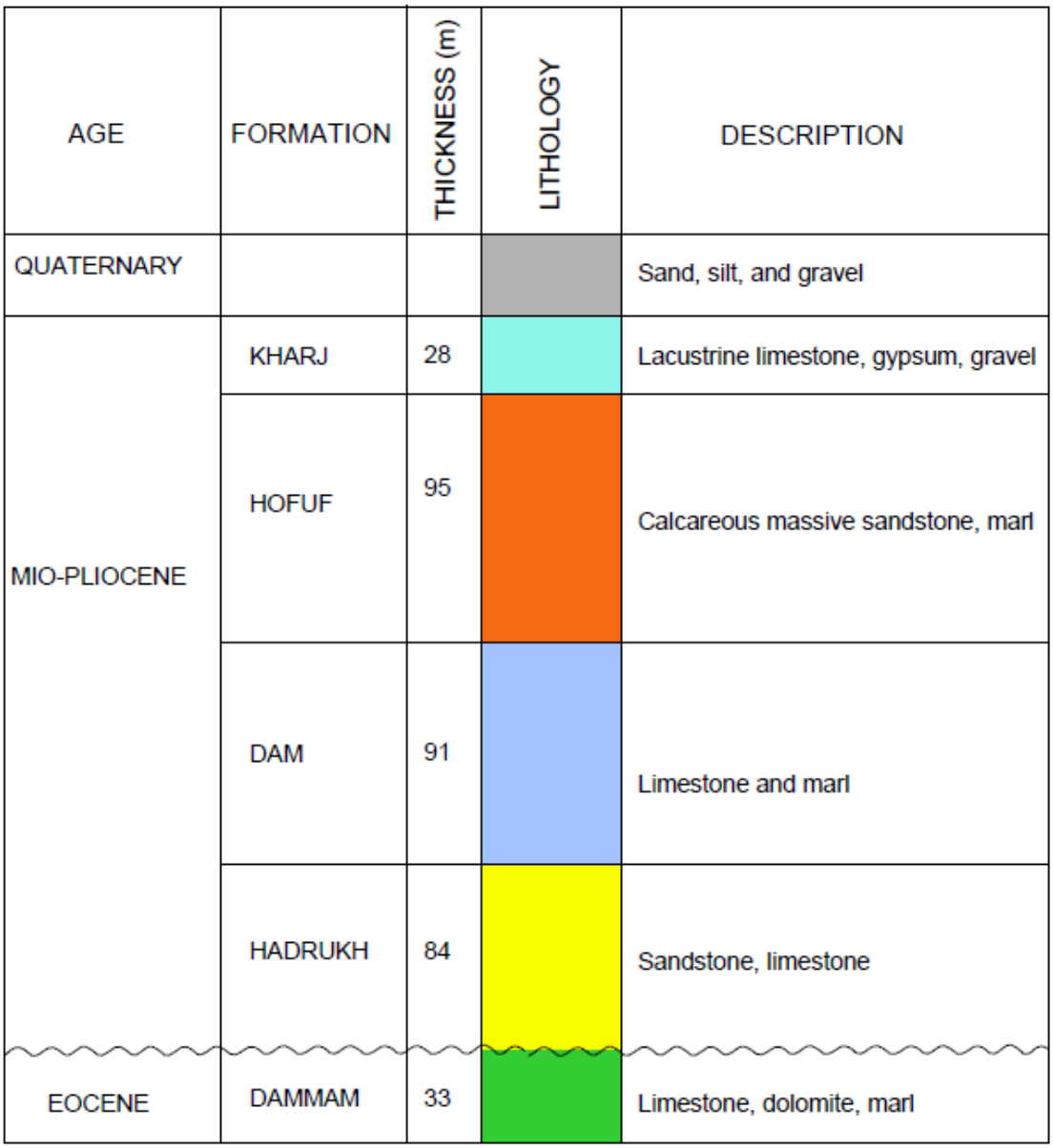

Figure 3: Generalized Stratigraphic Column of Ghawar area (Powers et al., 1966)

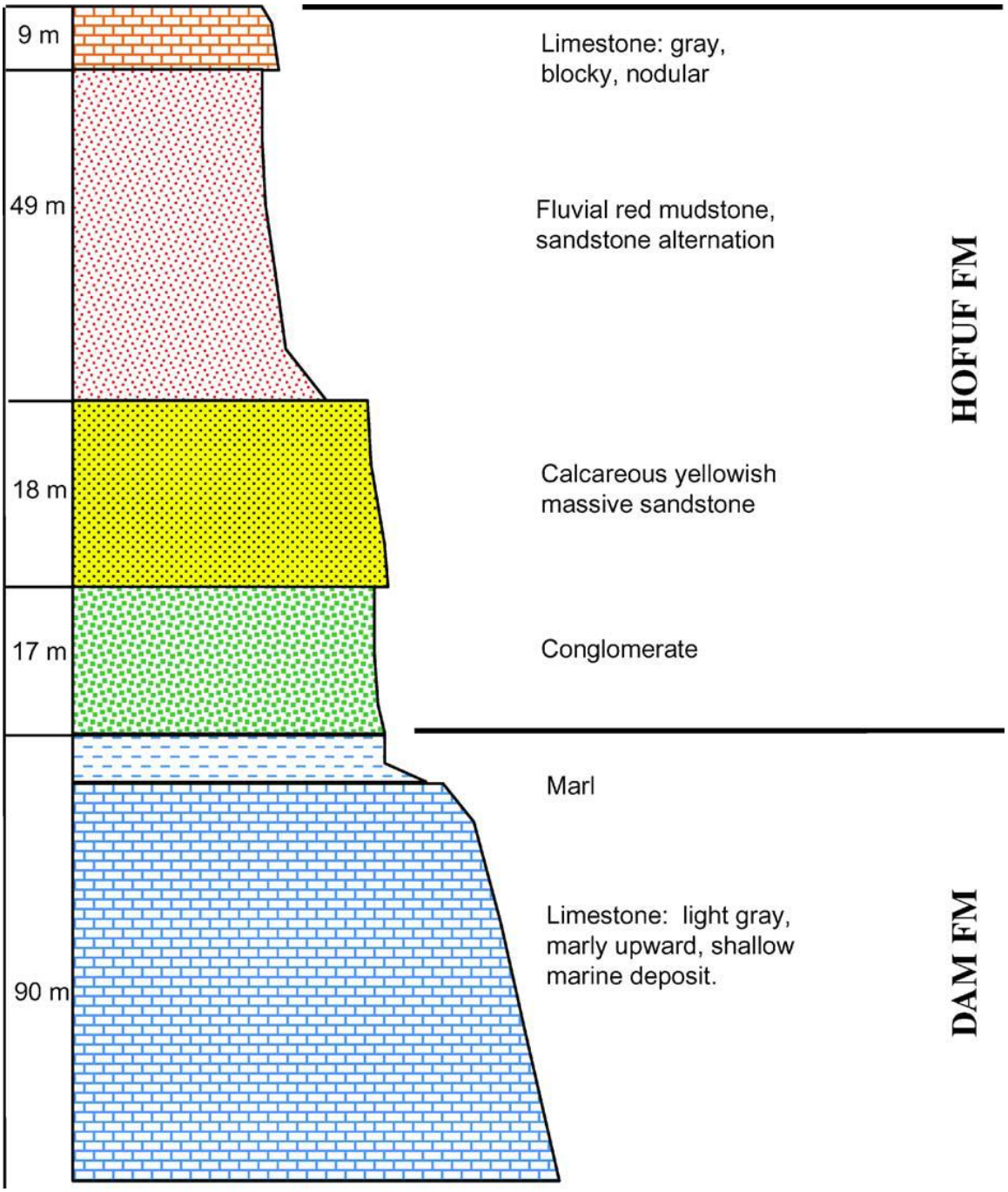

Figure 4: Stratigraphic column of Hofuf and Dam formations (Saner et al., 2005)

1.3 Problem Statement

Late Miocene-Early Pliocene Hofuf Formation is located in the eastern province, Saudi Arabia Figure 5. The aims of this study are to build outcrop models using and integrating sedimentology and image the subsurface through the Ground Penetrating Radar and Terrestrial Laser Scanning (LIDAR). Via sedimentology we will be able to come up with facies model that shows the distribution of vertically and laterally and another model which shows the distribution of the porosity estimated in the lab. Combining GPR data with LIDAR data would help to detect reflectors and interpret the GPR section. Finally, exporting these reflectors to LIDAR mesh point cloud will be the final model of the outcrop.

Figure 5: Hofuf Outcrop

CHAPTER 2

SEDIMENTOLOGY

2.1 Introduction

Three sampling sections were done along the outcrop vertical face with sampling interval 1m. Along each section we measured gamma ray Figure 6. The total number of samples is 31. Because Hofuf formation lithology is loose sandy and muddy in general (Saner et al., 2005), making plugs out of the samples were impossible. So, instead of plugs thin sections were made and then tested under microscope.

2.2 Outcrop Sections Description

2.2.1 First Section

In section 1 we have calcareous sandy mudstone with 5 % porosity. It has 20 % quartz. Then, sandstone sample has high porosity of 30%. Followed by mudstone with 3% porosity and it has something like dropstone. After that a sandy mudstone sample has 20% porosity. Again, another sandy mudstone sample has 15% porosity. Then, two siltstone samples the first one has 40% and 3% for the second one. For the first siltstone sample there is mudstone supported matrix. Then, a sandstone sample with 30% porosity. Two mudstone samples found with 2% porosity for the first one and 15%. The porosity for second one is associated with the grainy parts. Final sample was fine to medium sandstone sample with 10% porosity. Two cycles were noted in this section. The first one

starts by the sandstone at the bottom up to the mudstone with fine to medium sand. The second cycle starts from the siltstone up to the two mudstone layers. The total gamma ray for this section follows the facies but there is high gamma ray measurement for the second siltstone layer. I interpreted that the mud content in that siltstone sample is high and it is responsible for beside high gamma ray value the low porosity for that sample. Figure 7 summarizes the description of the first section.

Figure 6: Field work for Sampling and Gamma Ray

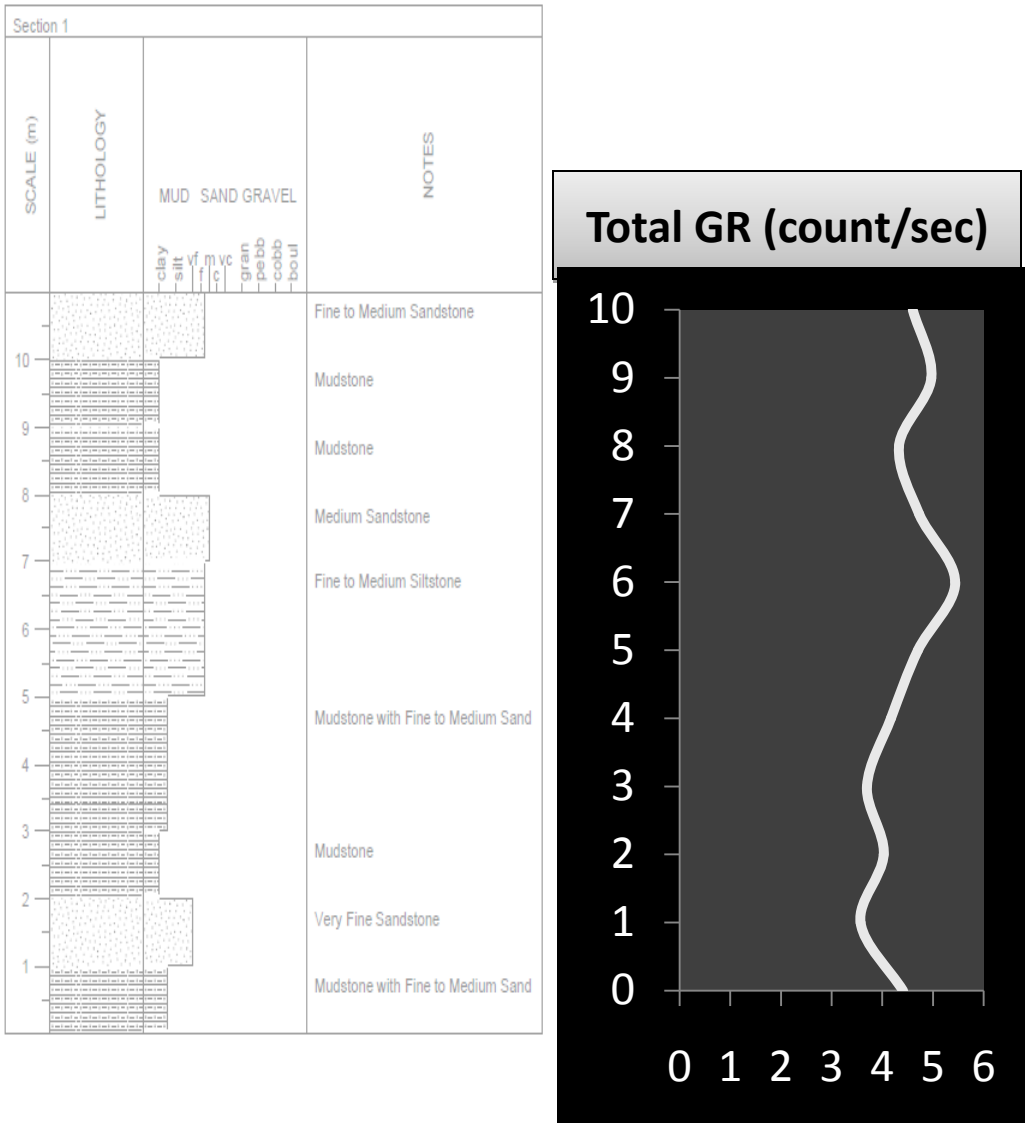

Figure 7: Section 1 shows Lithological Log and Total Gamma ray profile

2.2.2 Second Section

In section 2 we have medium to fine mudstone with 30 % porosity. Then, a silty mudstone sample has high porosity of 30%. Followed by fine to medium mudstone with 20% porosity and it has something like dropstone. Again, another silty mudstone sample found that has 2% porosity. Then, two very fine mudstone and silty mudstone samples were found the first one has 1% and almost 0% for the second one. Then, we have a sandy mudstone sample with 5% porosity. Two mudstone samples were found with 1% porosity for the first one and 2% for the second. The final two samples were silty mudstone with 10% porosity for the first one and 30% for the second one.

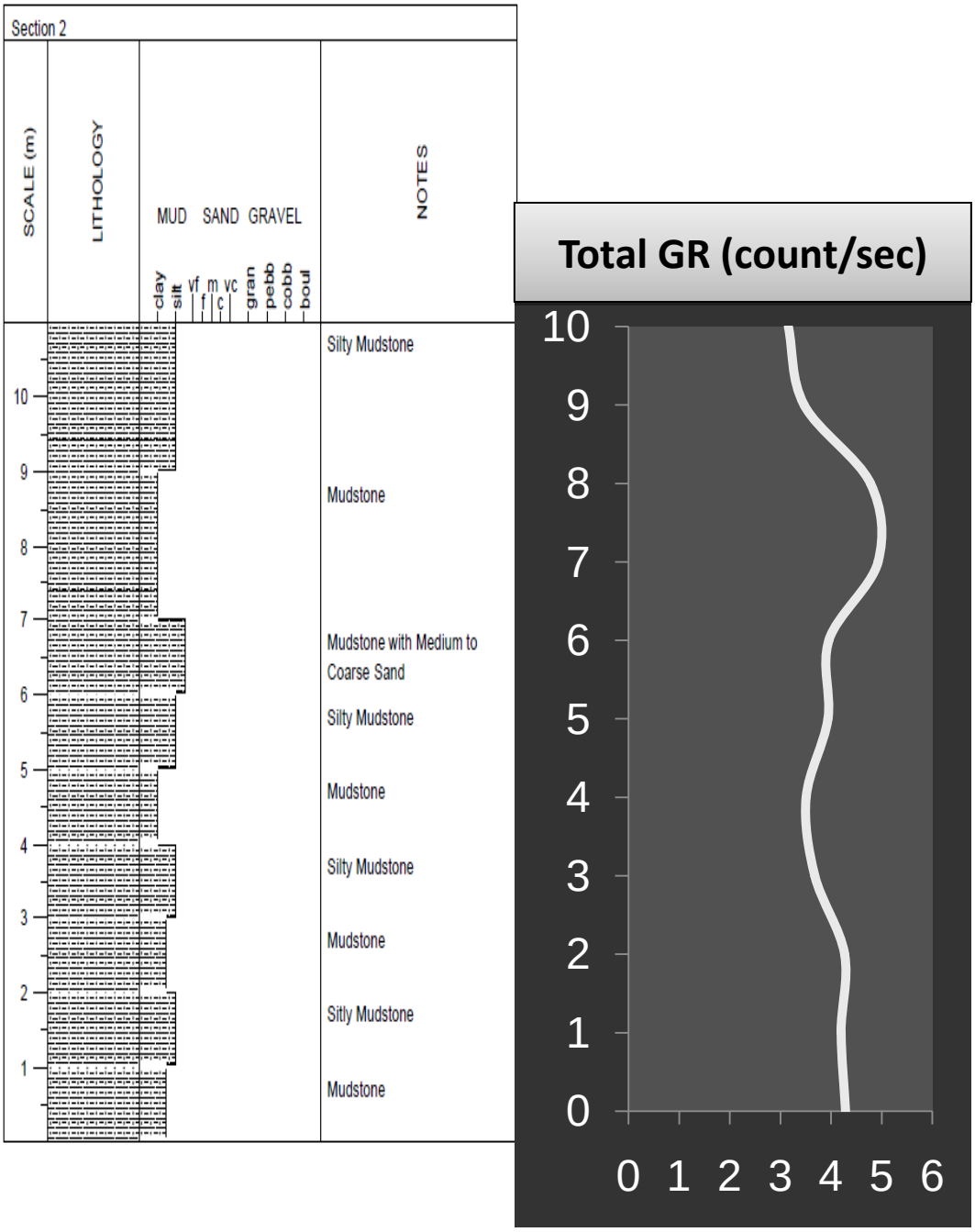

Figure 8: Section 2 shows Lithological Log and Total Gamma ray profile

2.2.3 Third Section

In section 3 we have only nine samples. The first was mudstone with almost 0 % porosity. Then, a silty mudstone sample has high porosity of 5%. Followed by fine to very fine sandy mudstone with 5% porosity. Again, three sandy mudstone samples found but they were medium to coarse. The first one has 40% porosity and the other two have 10% porosity. Then, two fine to medium mudstone samples found both have 10% porosity . The final sample was sandstone that has 15% porosity. Table 2summarizes the description of these samples.

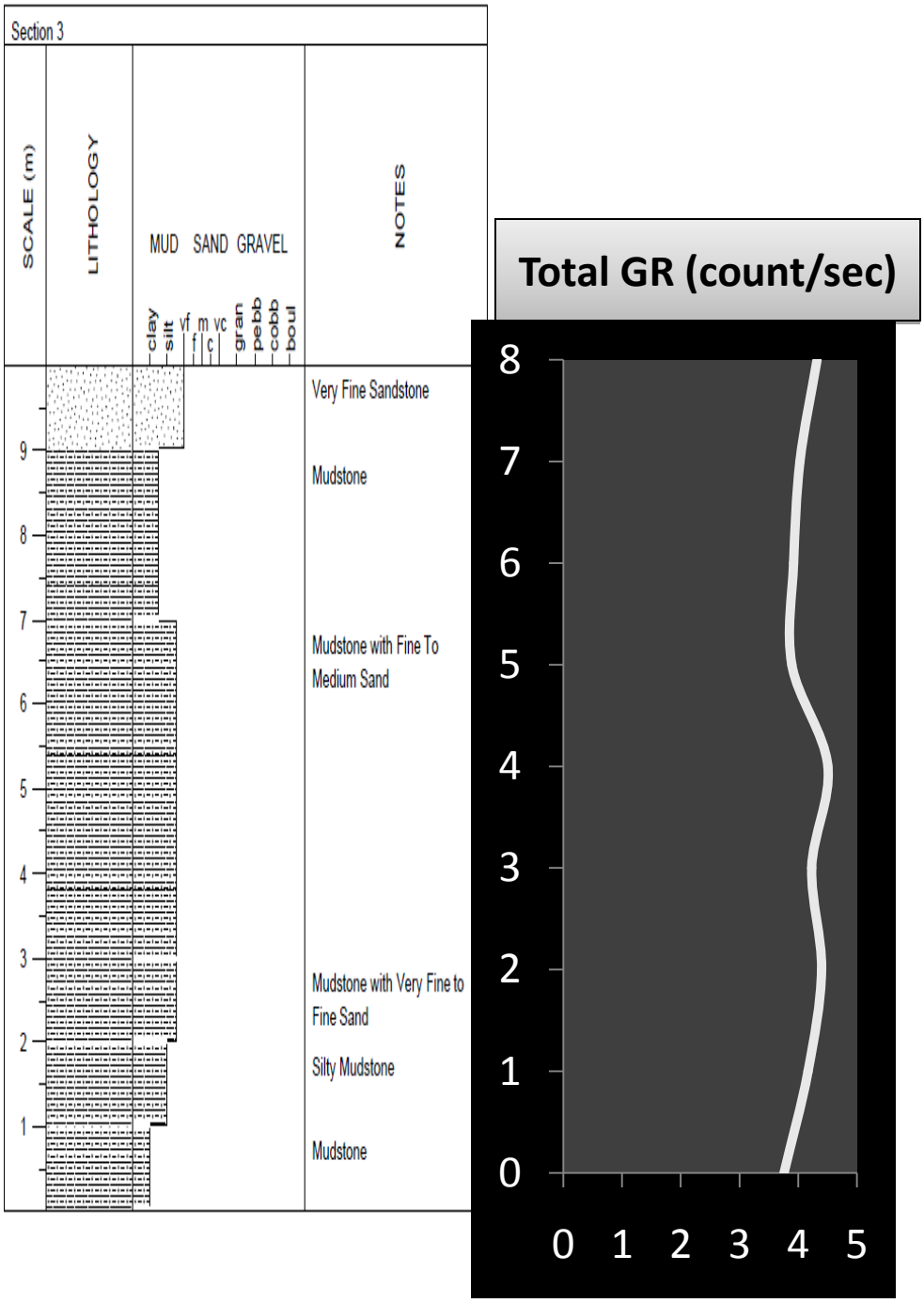

Figure 9: Section 3 shows Lithological Log and Total Gamma ray profile

Table 2: Porosity estimations, lithofacies and Gamma Ray

Section#	Sample#	Height (m)	Porosity (%)	Lithofacies	K_SGR	U_SGR	Th_SGR	Total GR
1	HS-1-1	1	5	sandy mudstone	3.17	0.97	0.27	4.41
	HS-1-2	2	30	sandstone	2.77	0.63	0.17	3.57
	HS-1-3	3	3	mudstone	3.03	0.77	0.23	4.03
	HS-1-4	4	20	mudstone	2.5	0.83	0.37	3.7
	HS-1-5	5	15	mudstone	2.73	1.07	0.37	4.17
	HS-1-6	6	40	siltstone	3.17	0.9	0.63	4.7
	HS-1-7	7	2	siltstone	3.6	1.07	0.77	5.44
	HS-1-8	8	30	sandstone	3.2	1.1	0.43	4.73
	HS-1-9	9	2	mudstone	2.9	0.9	0.53	4.33
	HS-1-10	10	15	mudstone	3.3	1.07	0.6	4.97
	HS-1-11	11	10	sandstone	3.2	0.93	0.47	4.6
2	HS-2-1	1	30	mudstone	2.98	0.92	0.39	4.29
	HS-2-2	2	30	silty mudstone	3.02	0.9	0.28	4.2
	HS-2-3	3	20	mudstone	3.09	0.89	0.29	4.27
	HS-2-4	4	2	silty mudstone	2.79	0.61	0.28	3.68
	HS-2-5	5	1	mudstone	2.75	0.58	0.18	3.51
	HS-2-6	6	0	silty mudstone	2.98	0.73	0.23	3.94
	HS-2-7	7	5	sandy mudstone	2.78	0.81	0.37	3.96
	HS-2-8	8	1	mudstone	3.64	1.09	0.2	4.93
	HS-2-9	9	2	mudstone	3.44	1.07	0.27	4.78
	HS-2-10	10	10	silty mudstone	2.7	0.6	0.17	3.47
	HS-2-11	11	30	silty mudstone	2.53	0.48	0.15	3.16
3	HS-3-1	1	0	mudstone	2.77	0.63	0.36	3.76
	HS-3-2	2	5	silty mudstone	2.79	1.11	0.27	4.17
	HS-3-3	3	5	sandy mudstone	2.84	1.15	0.41	4.4
	HS-3-4	4	40	sandy mudstone	3.01	0.96	0.26	4.23
	HS-3-5	5	10	sandy mudstone	3.185	0.85	0.28	4.505
	HS-3-6	6	10	sandy mudstone	2.61	0.87	0.41	3.89
	HS-3-7	7	10	mudstone	2.51	0.82	0.59	3.92
	HS-3-8	8	10	mudstone	3.07	0.79	0.28	4.03
	HS-3-9	9	15	sandstone	2.76	0.9	0.66	4.32

CHAPTER 3

Ground Penetrating Radar

Ground Penetrating Radar is the most important geophysical tool used in outcrop studies. Due to many reasons it has become more preferred than seismic in outcrop studies. One of these reasons is that seismic resolution cannot detect some thin target zones. Another issue is that there is no acoustic impedance contrast between sediment layers because of the cemented nature of sediments (Pringle, 2006). GPR overcomes these problems that seismic has and provide better image for outcrop due to its high resolution. Of course the depth of penetration of GPR is related to the frequency of the antenna. As the frequency of the antenna increases the depth of penetration decreases and vice versa. For our study an antenna with 100 MHZ frequency used to study theHofufoutcrop.

2.1 GPR Data Acquisition

The GPR survey was conducted in the second cliff of the outcrop. The first one the upper was excluded because of inaccessibility tothat part. The survey parameters are summarized in Table 3. After that, stations for DGPS data acquisition were marked along the GPR profile with distance of separation of 1.5 meter between stations Figure 11.

Figure 10: The 100 MHZ GPR Antenna

Table 3 : GPR Survey Parameters

100 MHZ Antenna	
Range	**500 ns**
Samples per Scan	**512**
Resolution	**16 bits**
Number of Gain Points	**5**
gain 1	**-20 dB**
gain 2	**10 dB**
gain 3	**20 dB**
gain 4	**30 dB**
gain 5	**40 dB**
Vertical High Pass	**30 MHZ**
Vertical low Pass	**200 MHZ**
Scans Per Second	**32**
Transmit Rate	**50 KHZ**
Dielectric	**4**

Figure 11: DGPS data acquisition

3.2 GPR Data Processing

After collecting the GPR data RADAN software was used for data processing. Figure 12 shows the raw field data before processing. The processing steps used were by order: Position Correction, Header Correction, Background Removal, Window Selection, Range Gain and Static Correction & Local Peaks. Each step will be discussed below.

3.2.1 Position Correction

Correct Position command found under Process in the toolbar. After choosing the command a window like the one shown below in Figure 13 will appear on the screen. The scan is displayed on the horizontal scale and an amplitude scale on the vertical one from 1 to -1.The small button shown on Delta Pos (ns) is used to make the scan to shift to the left until the first positive peak's left edge reaches to 0 in scan scale. Then a new file is saved Figure 14.

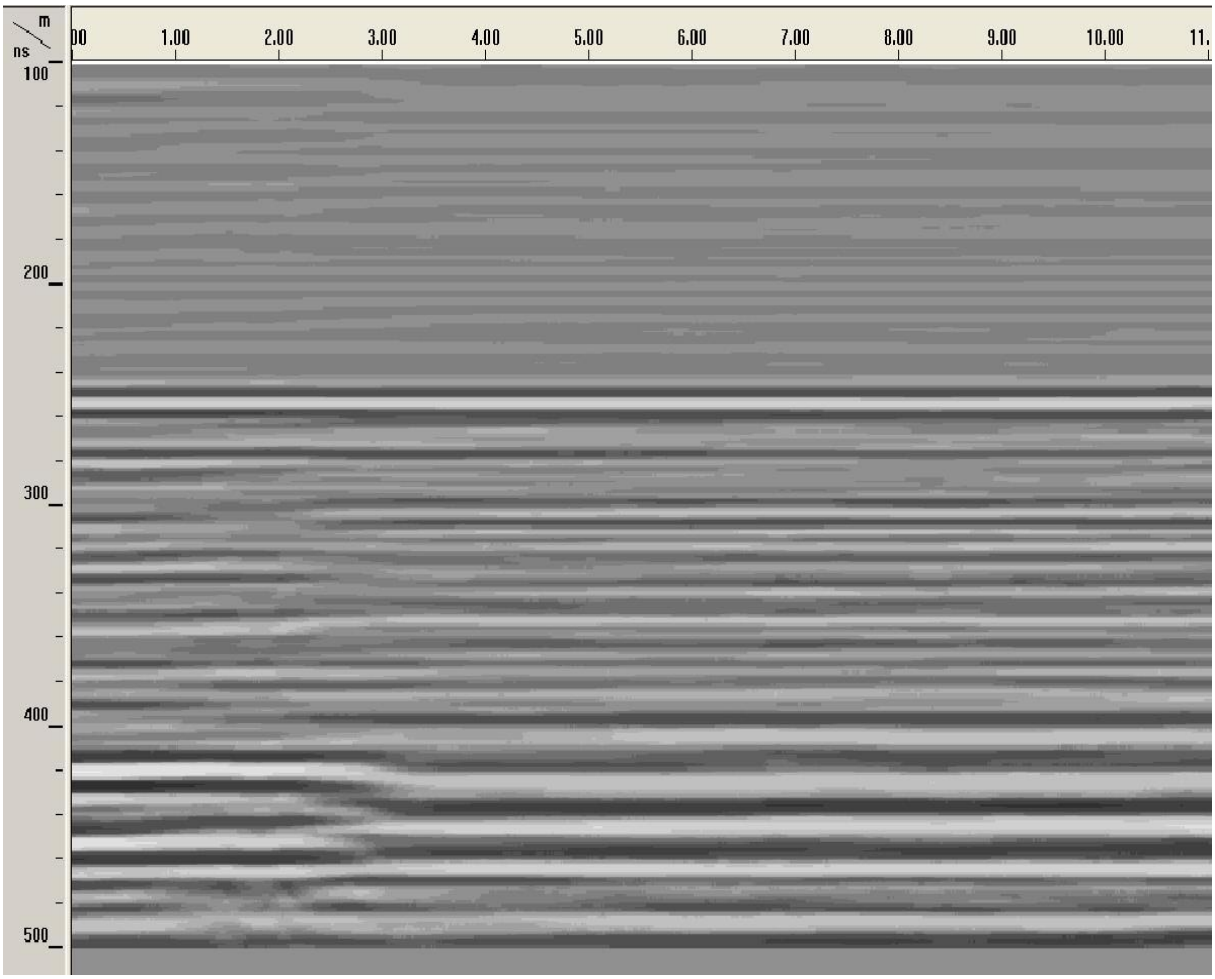

Figure 12: GPR Raw Data

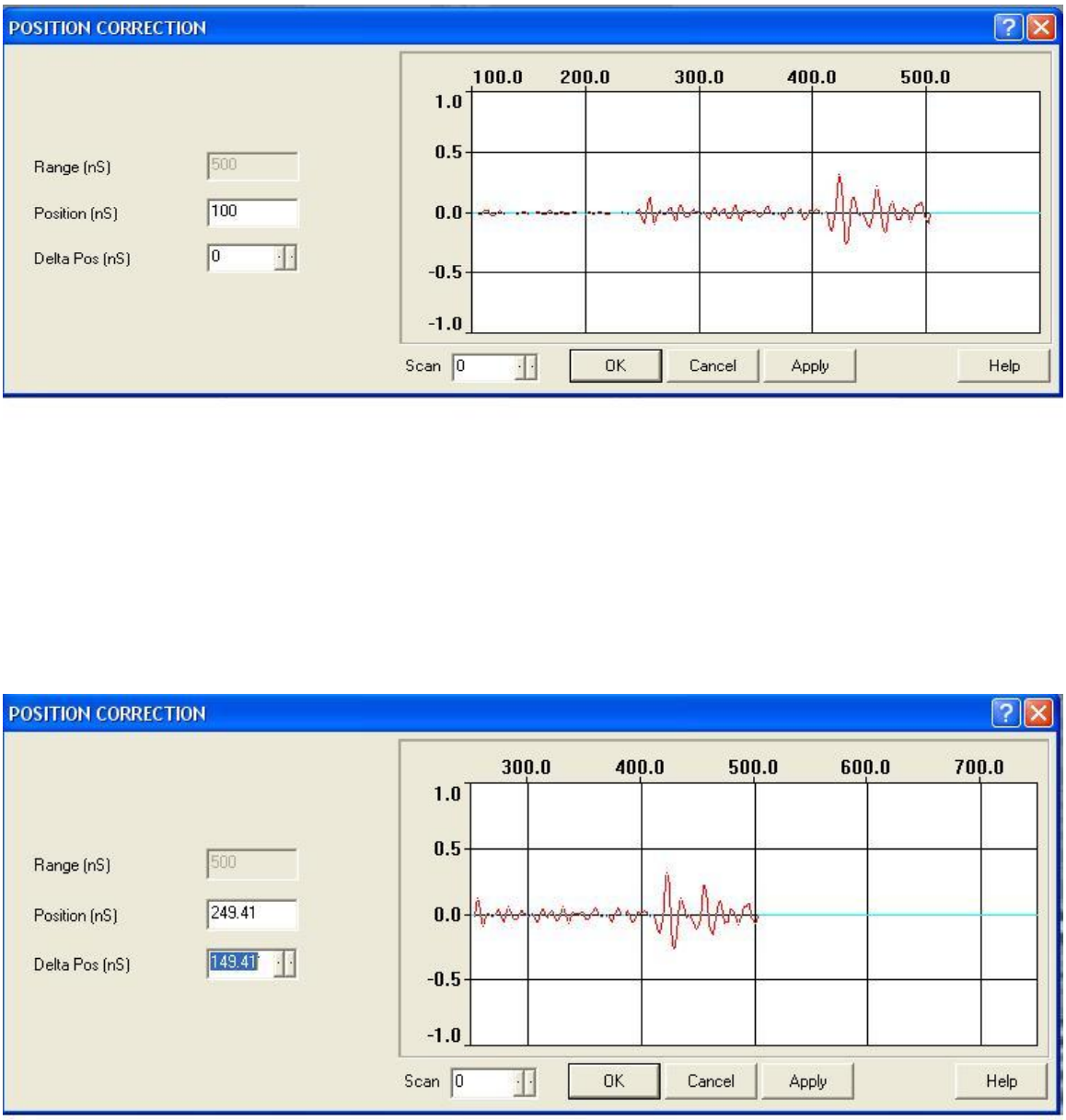

Figure 13: Top The Scan before shifting. Below after shifting

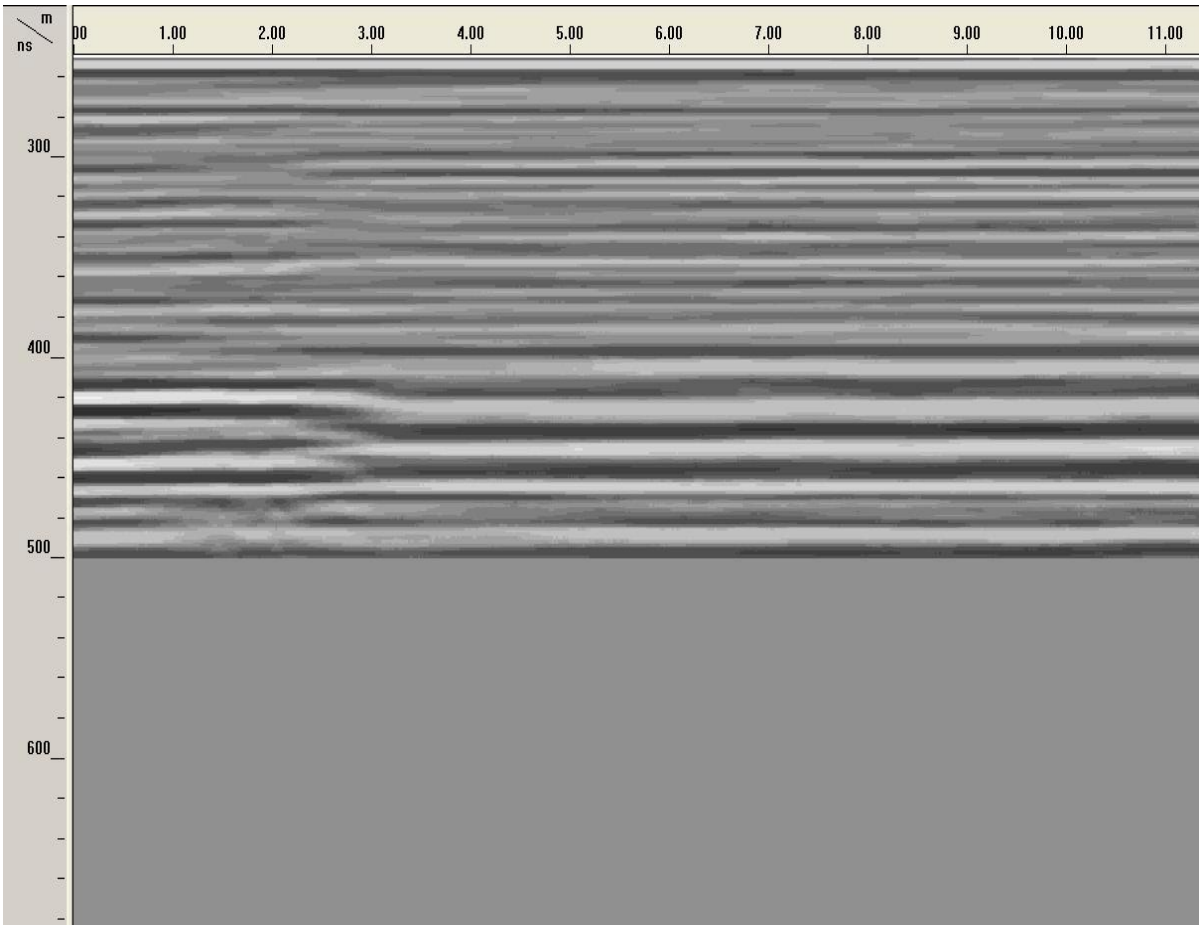

Figure 14: GPR Data after Position Correction

3.2.2 Header Correction

After Position Correction, some corrections in the header file have to be done. These corrections are done for Positions (ns) and scans/m Figure 15.

3.2.3 Background Removal

Background removal is a form of spatial filtering; most often, a kind of a high pass filter. Background filter can eliminate temporally consistent noise from the data which helps the real signals that were previously covered by this noise to be more visible. This can be accomplished by the following steps:

1) Under Process in the toolbar FIR Filter command was chosen and a window will show up.
2) Background removal (scans) is changed from 0 to 1023 and then the filter is applied Figure 16.
3) A new data after filtering will appear and can be saved Figure 17.

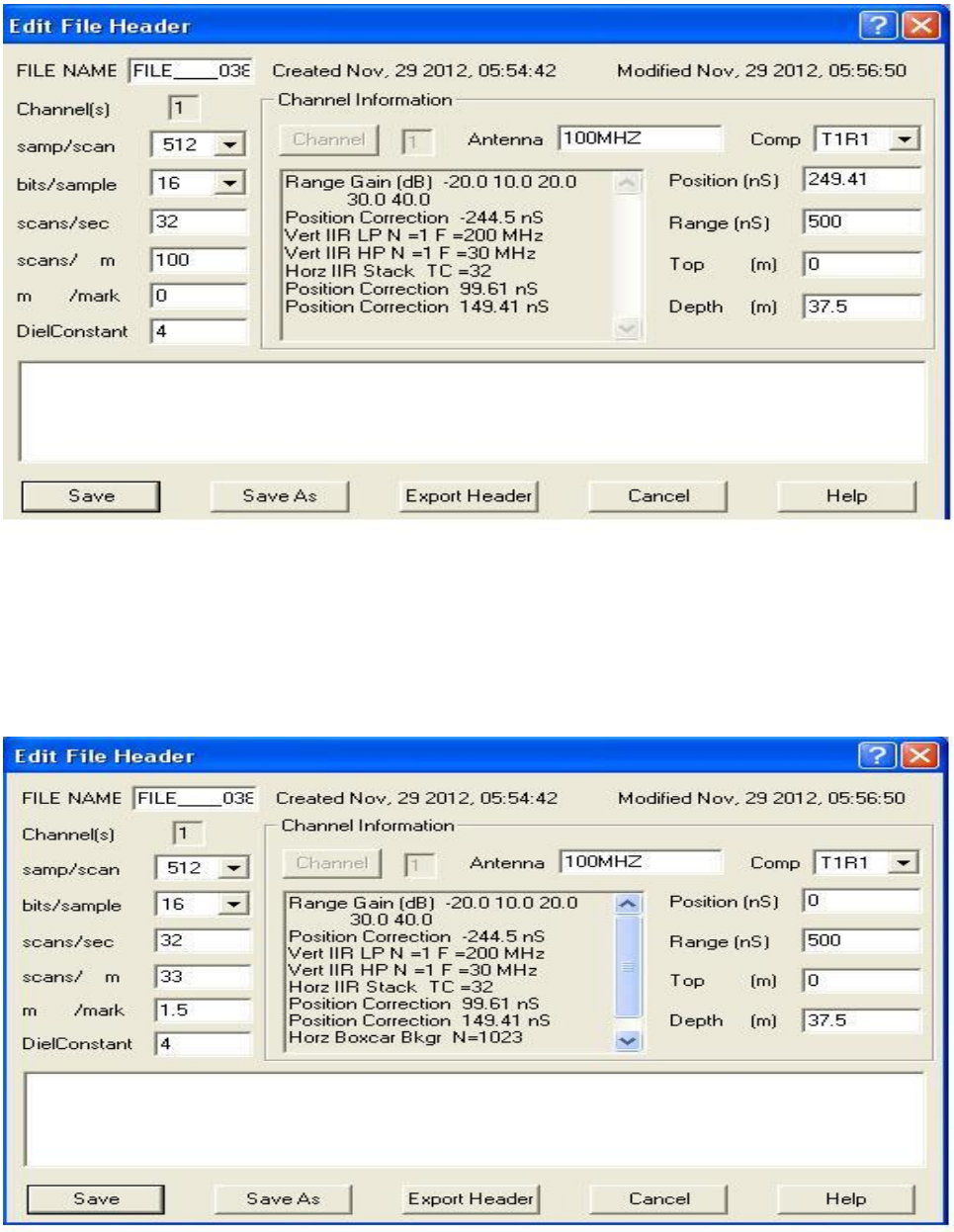

Figure 15: Header Correction before (top) and after (below)

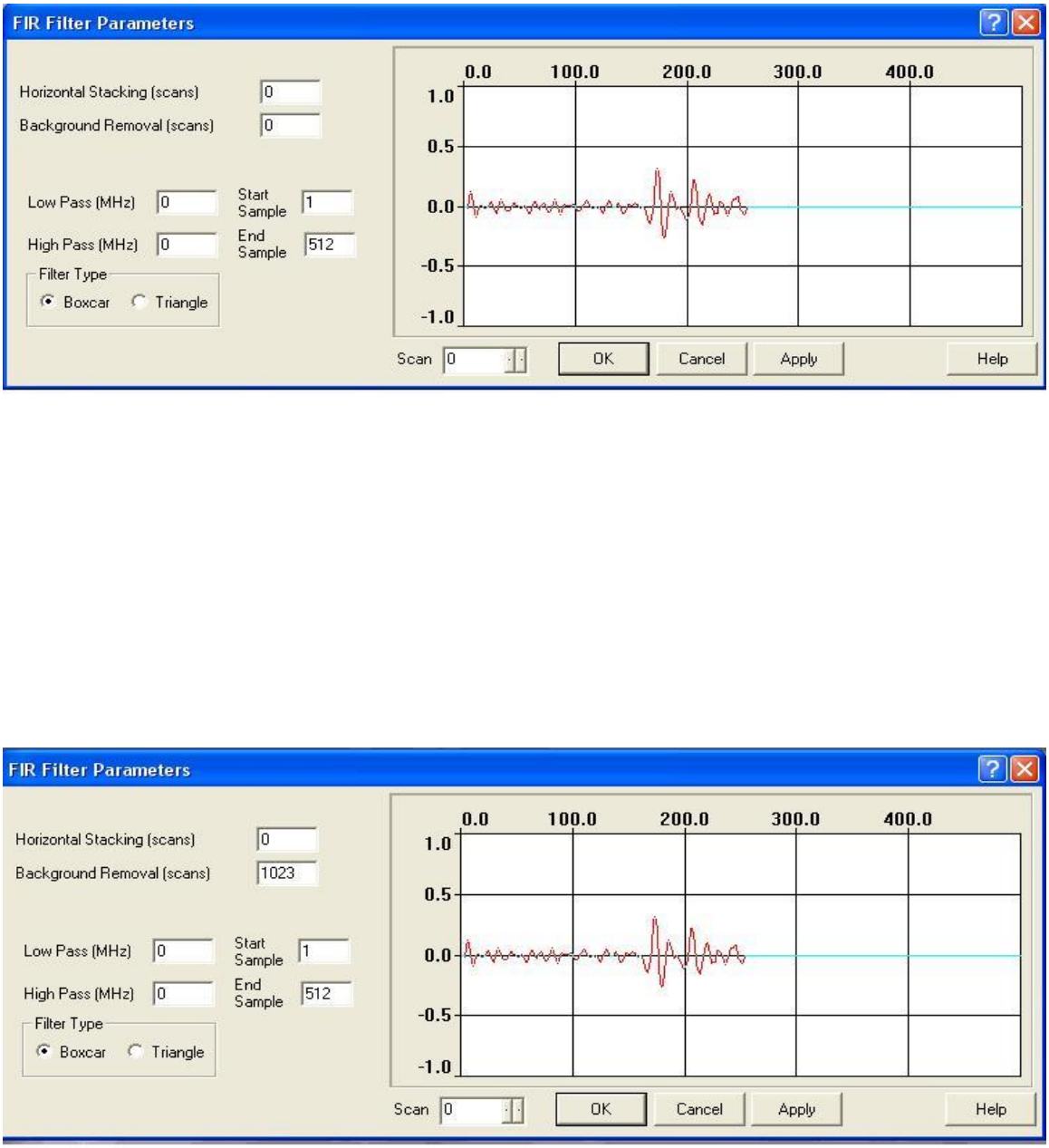

Figure 16: FIR Filter window

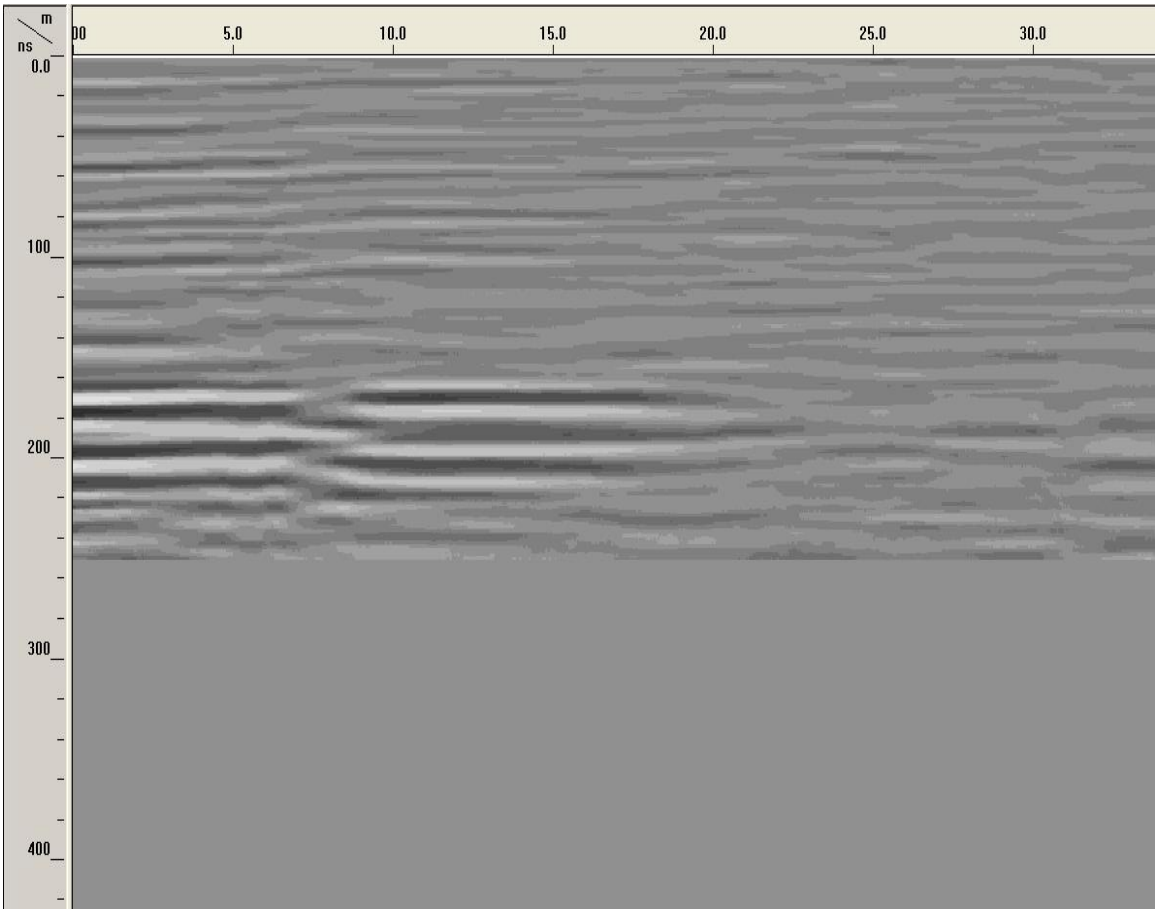

Figure 17: GPR data after FIR Filter

3.2.4 Window Selection

As mentioned in the previous chapter the three sections of sampling are located inside the GPR profile. We need to select the area in the profile that somehow starts and ends with the two geological sections at the edges. We have the DGPS along the GPR profile and we have the DGPS data for each section. We will use the following formula for calculating the distance

$$\mathrm{d} = \sqrt{(X_1 - X_2)^2 + (Y_1 - Y_2)^2 + (Z_1 - Z_2)^2} \quad (1.1)$$

The points used are the three points related to the sampling sections and the first point of the GPR profile. The distance will be between each one of the three points and the first point in the profile. Table 4shows the distances between these points. Now we can calculate the number of scans related to desired distances.

Now from the toolbar menu we will choose EDITand then SELECT. A window will appear Figure 18 asking for selecting a window depending on starting scan number and the ending scan number. From the header the scans/m equals to 33. The window will be chosen to start before and end after the two sections at the edges. For starting scan we will choose D to be 24 meter and for the ending scan D will be 92 meter.

$$\mathrm{Scan} = \mathrm{Distance} * (\frac{\mathrm{scan}}{\mathrm{m}}) \quad (1.1)$$

So the values are :

Starting scan = 792

Ending scan = 3036

Table 4 : Distances between Sampling sections and First point in GPR data

	X (m)	Y (m)	Z (m)	D (m)
First Point	347716.634	2839644.245	203.376	91.6239106
Section 1	347656.369	2839713.133	207.561	
First Point	347716.634	2839644.245	203.376	66.55918197
Section 2	347675.088	2839696.155	206.443	
First Point	347716.634	2839644.245	203.376	26.07275003
section 3	347703.531	2839666.687	205.487	

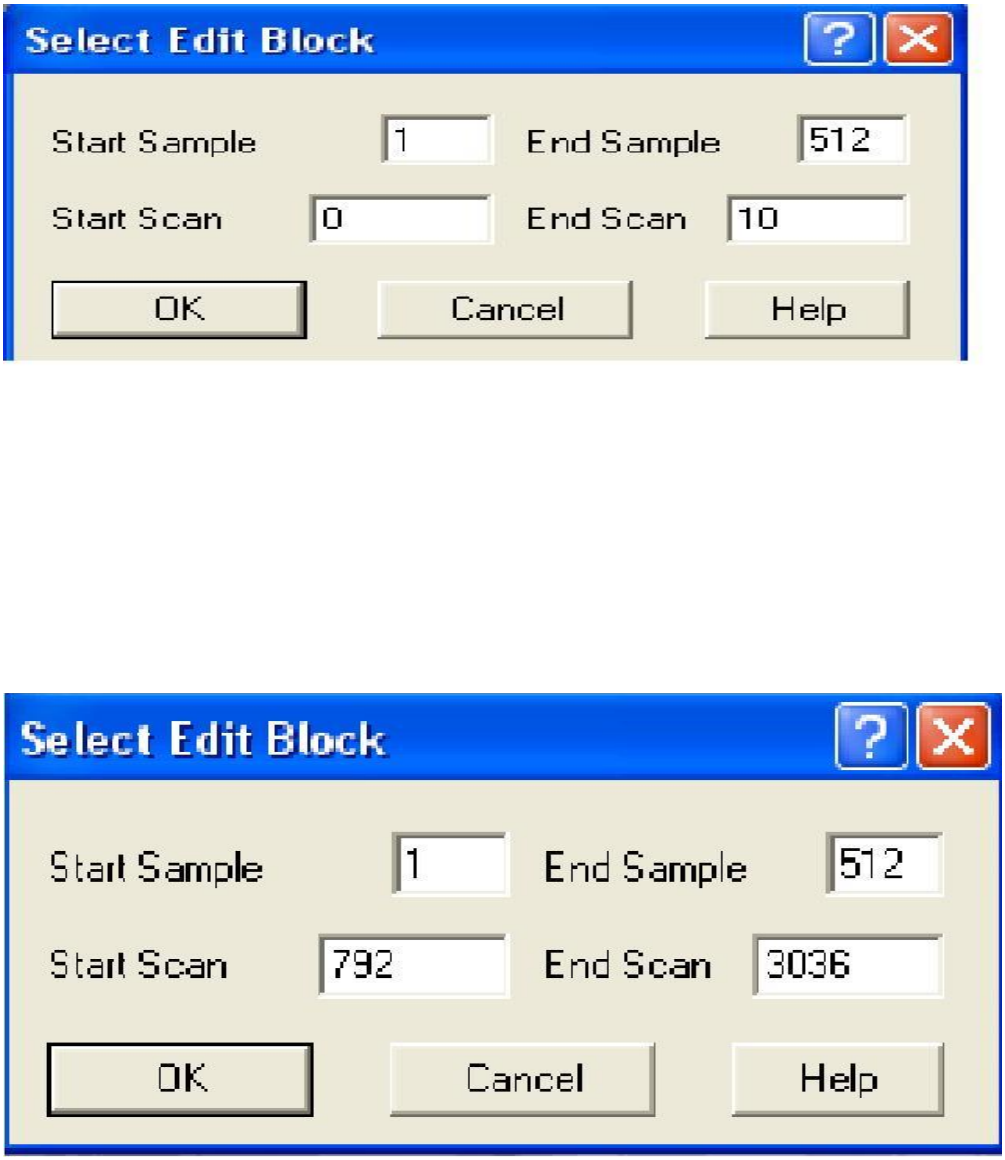

Figure 18: Select Window before (top) and after (below)

3.2.5 Gain Range

Gain is used to enhance weak signals or reflections. The gain command again is found under PROCESS in the toolbar. After choosing the range gain a window appears. The type of gain can be chosen between exponential or automatic one. The two types were applied to the section that was selected from the data and the exponential gain seems working better than automatic Figure 19.

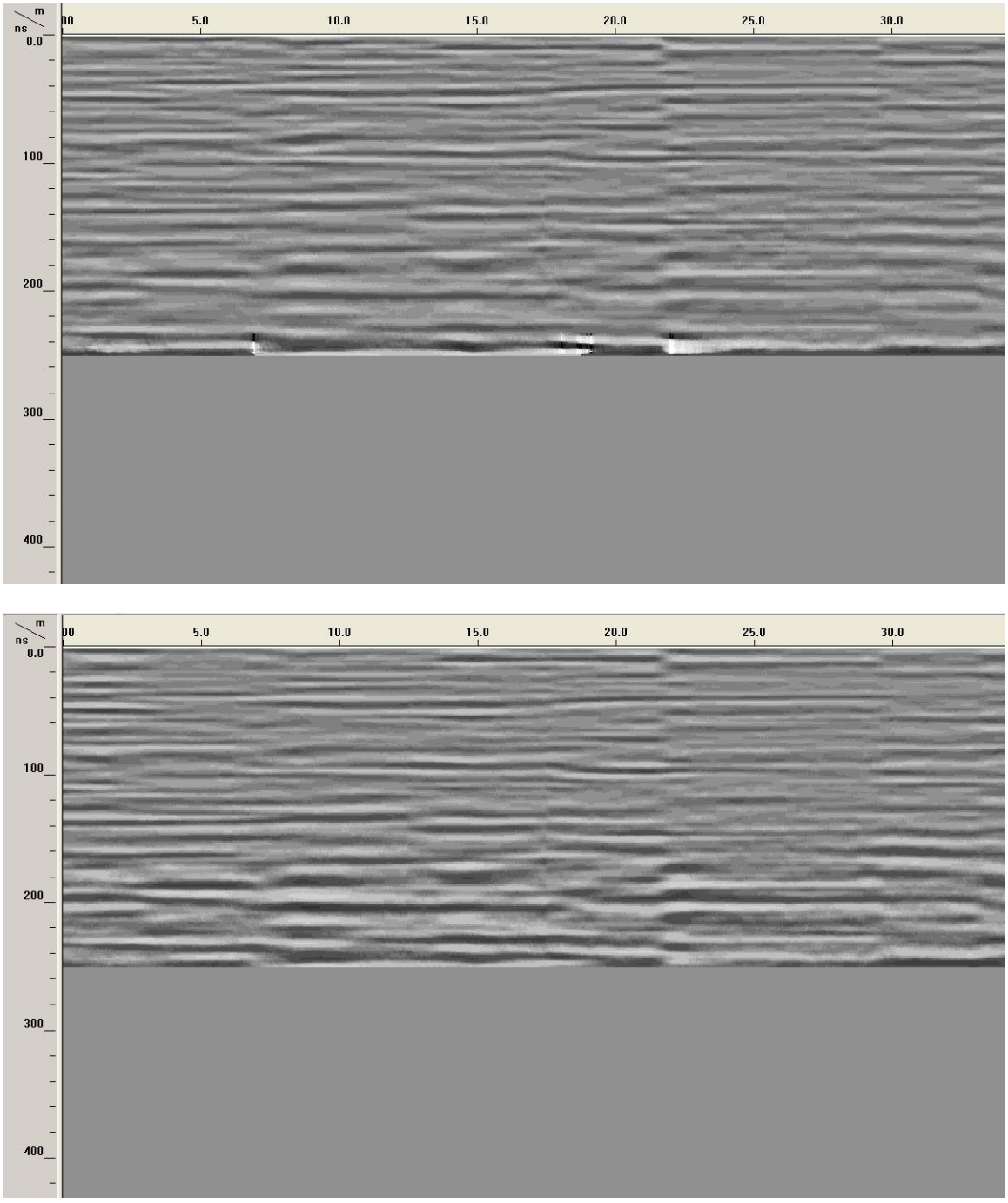

Figure 19: (top) Automatic Gain. (below) Exp. Gain

3.2.6 Static Correction & Local Peaks

Static correction deals with the correction in the variation in elevation. To approach this correction, Differential GPS readings were collected along the GPR profile. The space between GPS stations was 1.5 m.

Local Peaks command is used to trace automatically continuous reflections in the data. After selecting the LOCAL PEAKS command from PROCESS in the toolbar, a dialog box will appear to select the appropriate parameters Figure 20. These parameters are :

1) Max # of Points: indicates the number of peaks to trace.

2) Sample/Point: represents the width of the peak in the vertical direction.

3) Start and End Samples:Allows the user to decide the starting position of the file and the desired end if the user focuses on a specific zone instead of selecting the whole file.

Figure 21 shows the final result of static correction and Local Peaks.

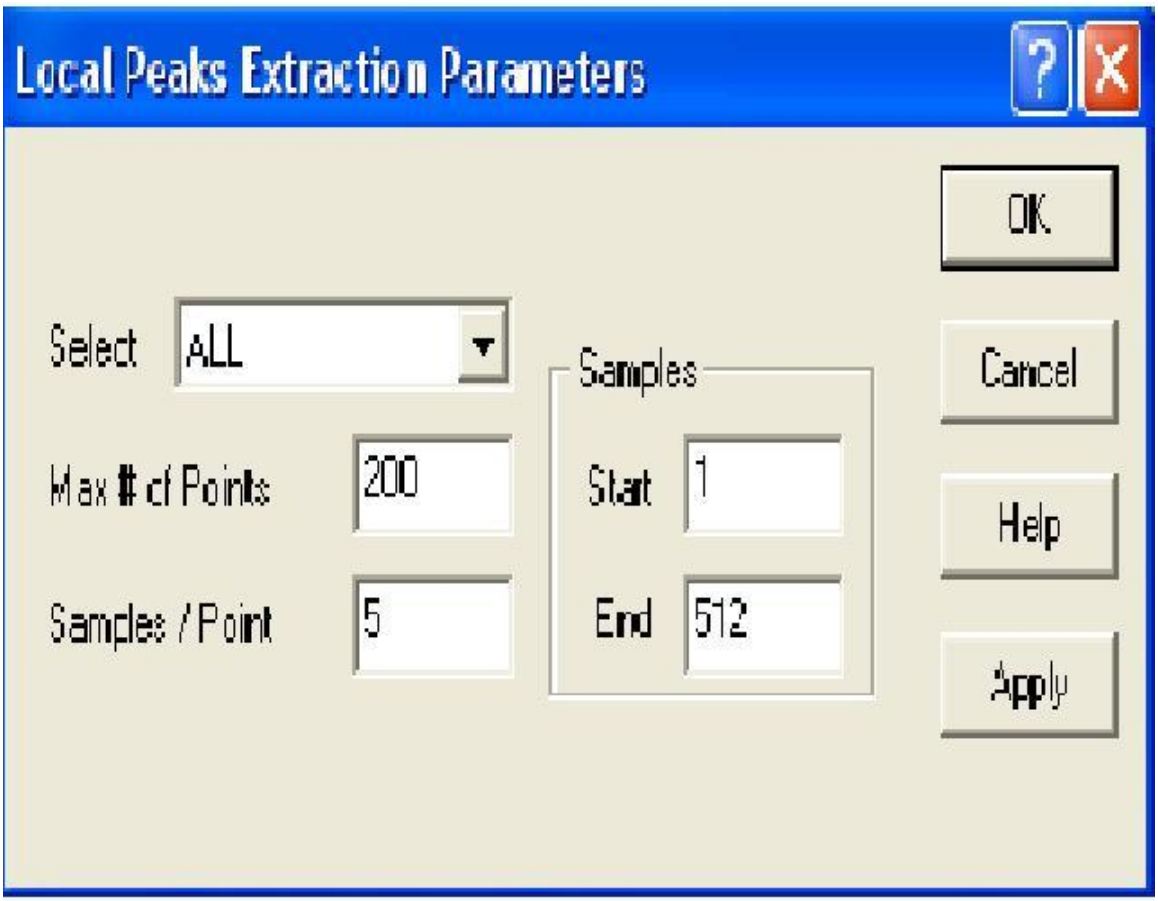

Figure 20: Local Peaks Parameters

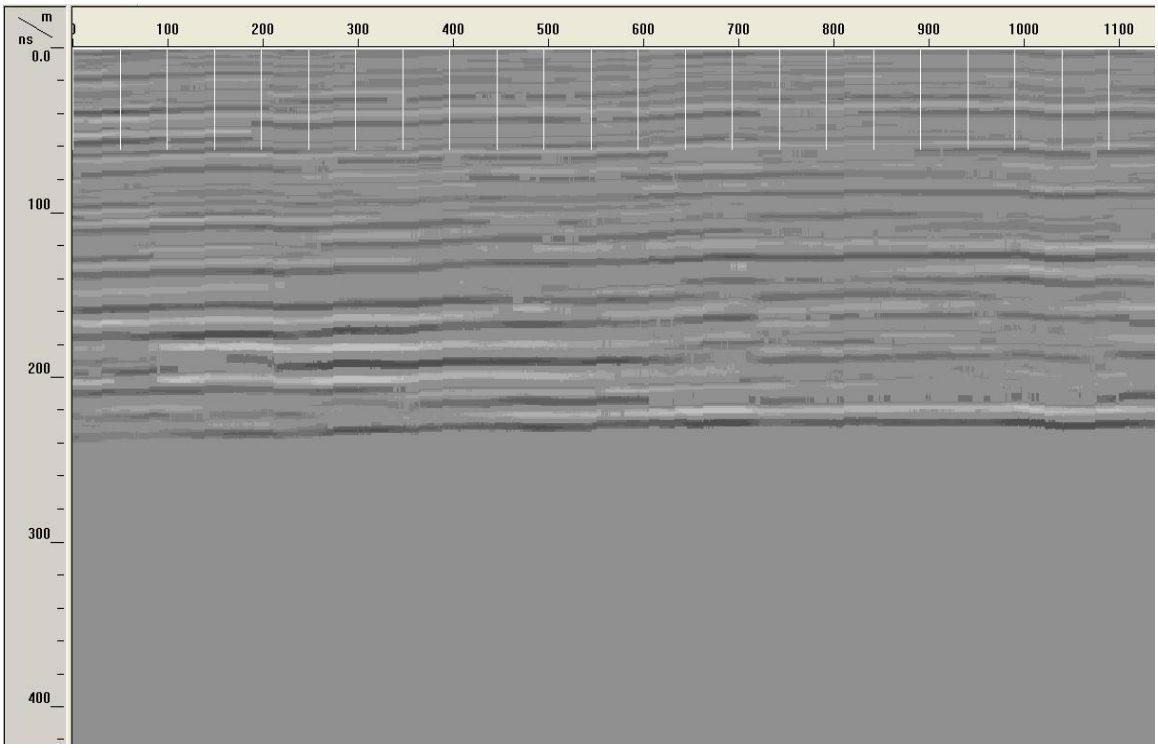

Figure 21: GPR data after static correction & local peaks

CHAPTER 4

Terrestrial Laser Scanning (LIDAR)

Terrestrial laser scanning or LIDAR is one of the most preferable and accurate methodsin outcrop studies. 2D and 3D images of the outcrop can be acquired and processed via LIDAR. Normal workflow of LIDAR data acquisition and processing is shown in Figure 22. In this work a 2D LIDAR image of Hofuf outcrop wasacquired and processed.

4.1 LIDAR Data Acquisition

Four positions were selected for the survey. For all positions the following steps were applied:

1) Connect the control unit (Laptop or PAD) to the scanner via Ethernet cable or wireless.

2) Set the camera (Internal camera or an external one).

3) Select the area to be scanned (arrow eye).

4) Define the resolution.

5) Select data destination and start scanning.

At the end of the scanning I got four point clouds for the outcrop from different positions.

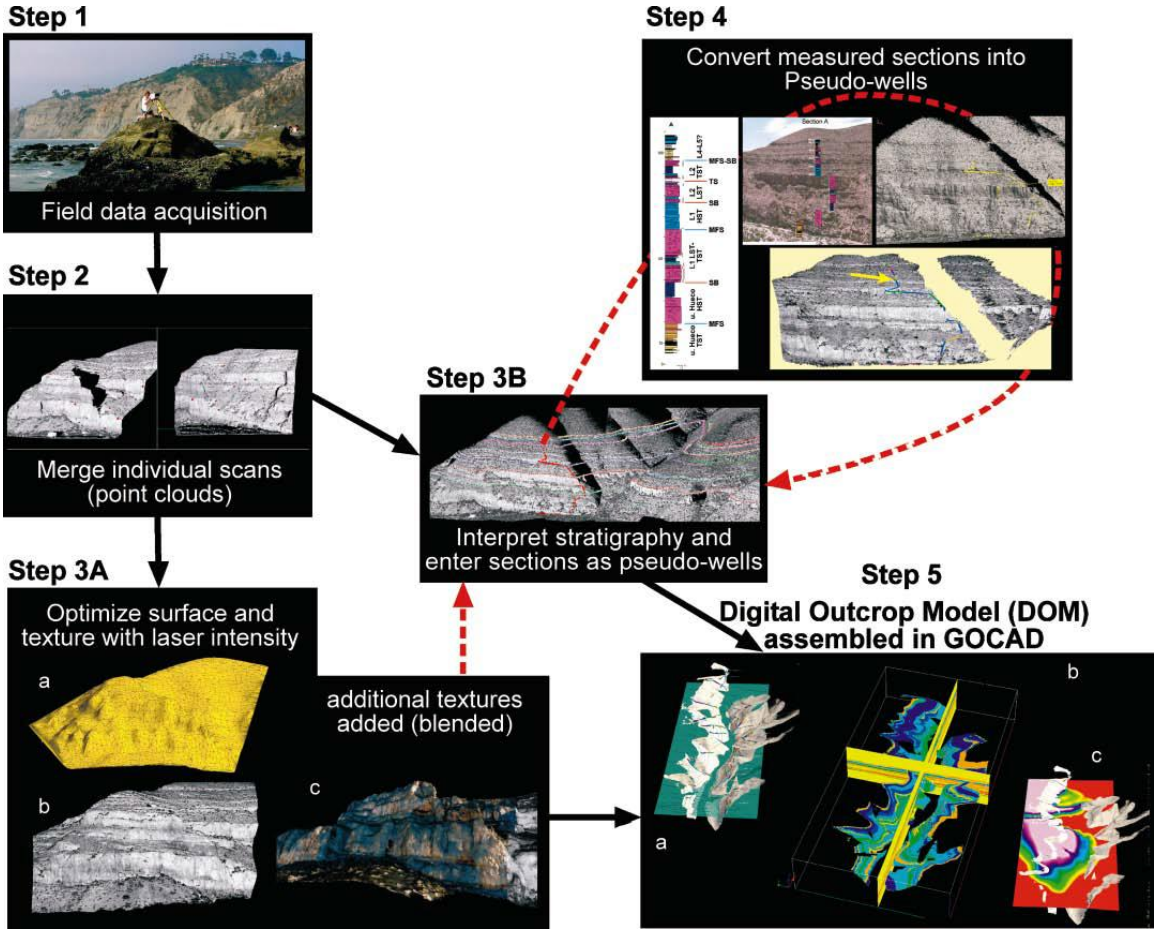

Figure 22: LIDAR workflow (Bellian et al., 2005)

4.2 LIDAR Data Processing

The first step in LIDAR data processing is to insert the data into Parcer. Via Parcer the data will be colored by adding texture image captured by internal or external camera. Then, save the data as Polyworks format to use it in Polyworks software. Because we have four point clouds, we have to merge them into one point cloud. The four point clouds will be added to IMAlign software inside Polyworks. Two point clouds will be merged first by selecting several common points for them. This step will be repeated for the remaining point clouds and finally we will end up with a full single point cloud for the face of the outcrop Figure 24. Next step is to load the new data into IMSurvey. If inside IMSurvey we notice empty parts of the scan that happens because the laser beam did not reach to that part. Mesh is created to fill the gaps so that the data can be used later as a full model without gaps in the final part of the work.

Figure 23: LIDAR Data Processing From Parcer to IMAlign

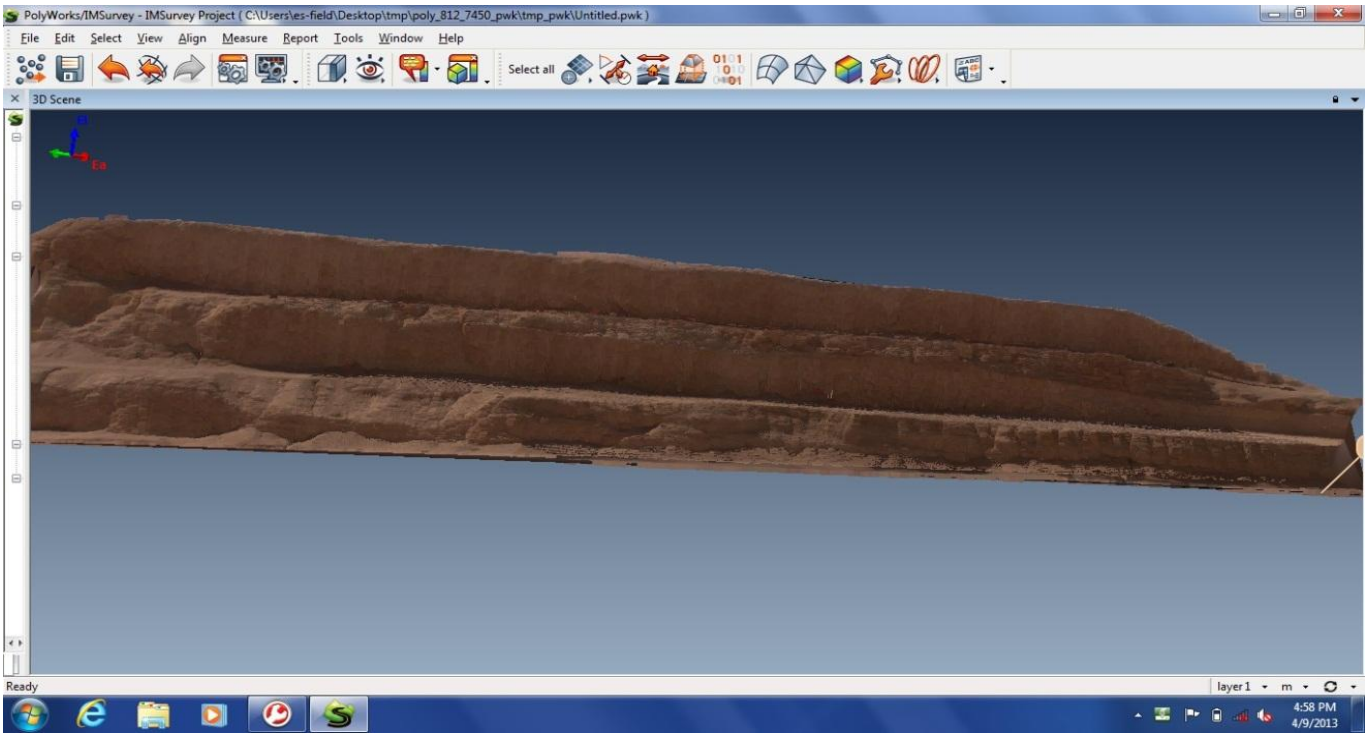

Figure 24: Full point cloud of outcrop after merging and coloring

CHAPTER 5

Data Analysis & Integration

In this chapter I will discuss and analyze the results I got from ground penetrating radar, LIDAR and sedimentology. The three columns were constructed from sampling used in building porosity and facies models Figure 25.The areas indicates high porosity values associated with sandstone as the facies model shows. On the other hand the areas with low porosity values areassociated with the existence of mudstone. Overall, the model shows low porosity values and by referring to the facies model we can see that mudstone is dominant. From this model we can alsosay that this part of Hofuf formation that is exposed in this area is within the part of fluvial red mudstone sandstone alteration in the geological column of the formation Figure 4. Also, this part of Hofuf formation shows a fluvial depositional environment and was deposited in meandering stream.

Ground penetrating radar and LIDAR were integrated in detecting the reflectors. I detected the reflector in the GPR profile and then lookedfor that reflector in the LIDAR point cloud. This kind of method integrates GPR profile with an image for the face of the outcrop (Zeng, et al., 2004;Franseen, et al., 2007; LEE, et al., 2007). Another method is to use high resolution facies models to interpret GPR profiles (Ruffell, et al., 2004). Here instead of facies model and images we will use the LIDAR point cloud. From the last processed GPR profile we can notice that the depth of penetration is larger than the outcrop thickness. Six reflectors in the GPR section weredetected within the range of the outcrop thickness and the seventh one is beyond the thickness of the outcrop. There are

some small reflectors scattered along the GPR section and they appeared in some areas and disappeared in others and that due to the variation in the mud content which is responsible for the contrast that makes the reflectors. The first reflector shows the boundary between the sandstone at the top and the mudstone below it. The second and third reflectors are associated with boundaries between the mudstone and sandstone for the second reflector and between siltstone and mudstone below it. However, there is a reflector lies between the second and the third reflector within the siltstone layer. I think this reflector appeared in this part although there should be no contrast between the sandstone and the siltstone below it. By going back to lithofacies log and total gamma ray profile for section 1 Figure 7I can see that the mud content in the siltstone sample is high and it is associated with the low porosity of that sample. The fourth and fifth reflectors showthe boundaries between the sandstone and mudstone above and below it. In LIDAR point cloud I could track three reflectors (2^{nd}, 3^{rd}& 4^{th}). These reflectors were marked in the point cloud as polylines in the IMSurveyFigure 27. These polylines can be exported and then use them to mark the position of the reflectors in the mesh model Figure 28.

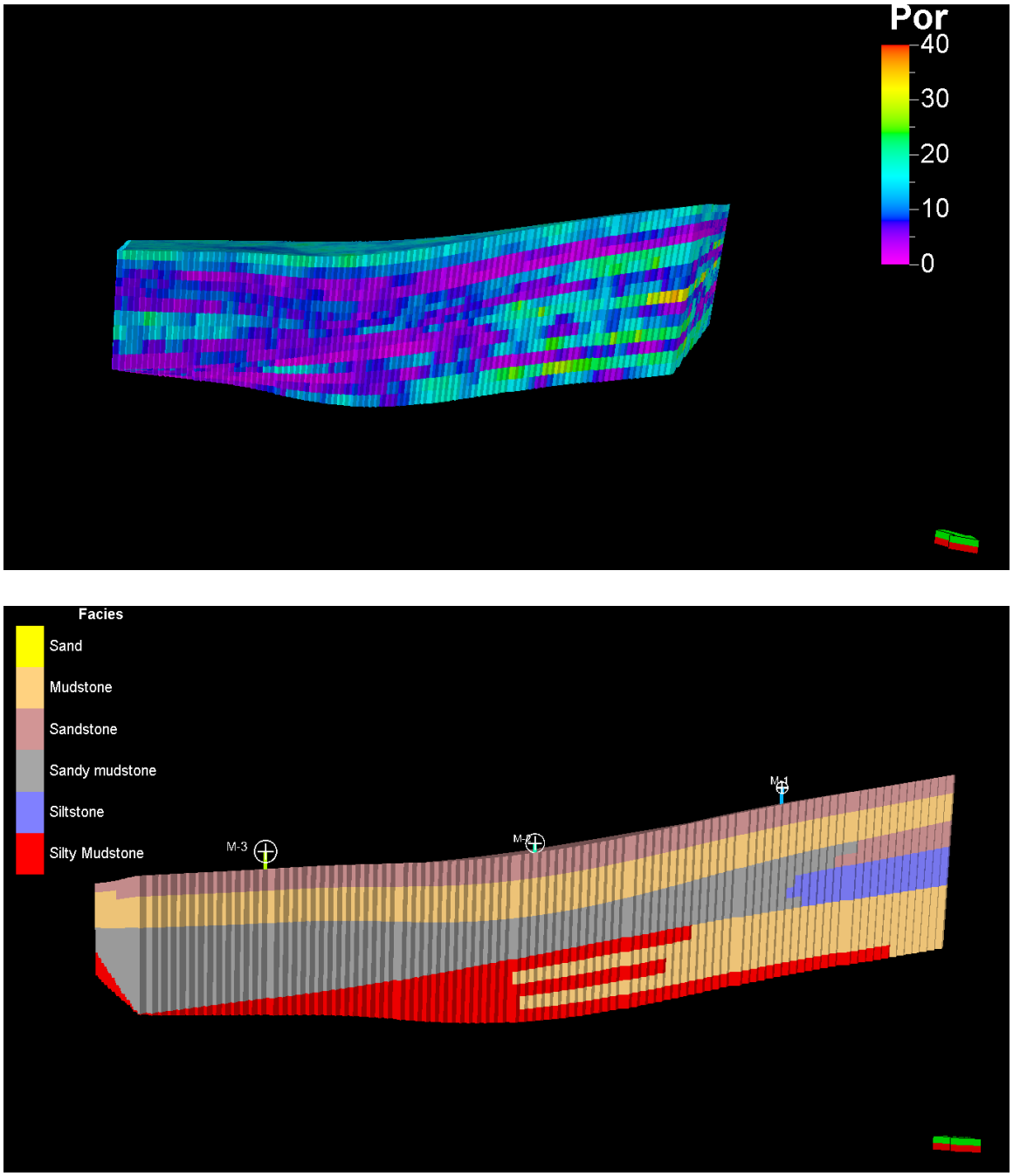

Figure 25: Porosity Model (top) and Facis Model (bottom)

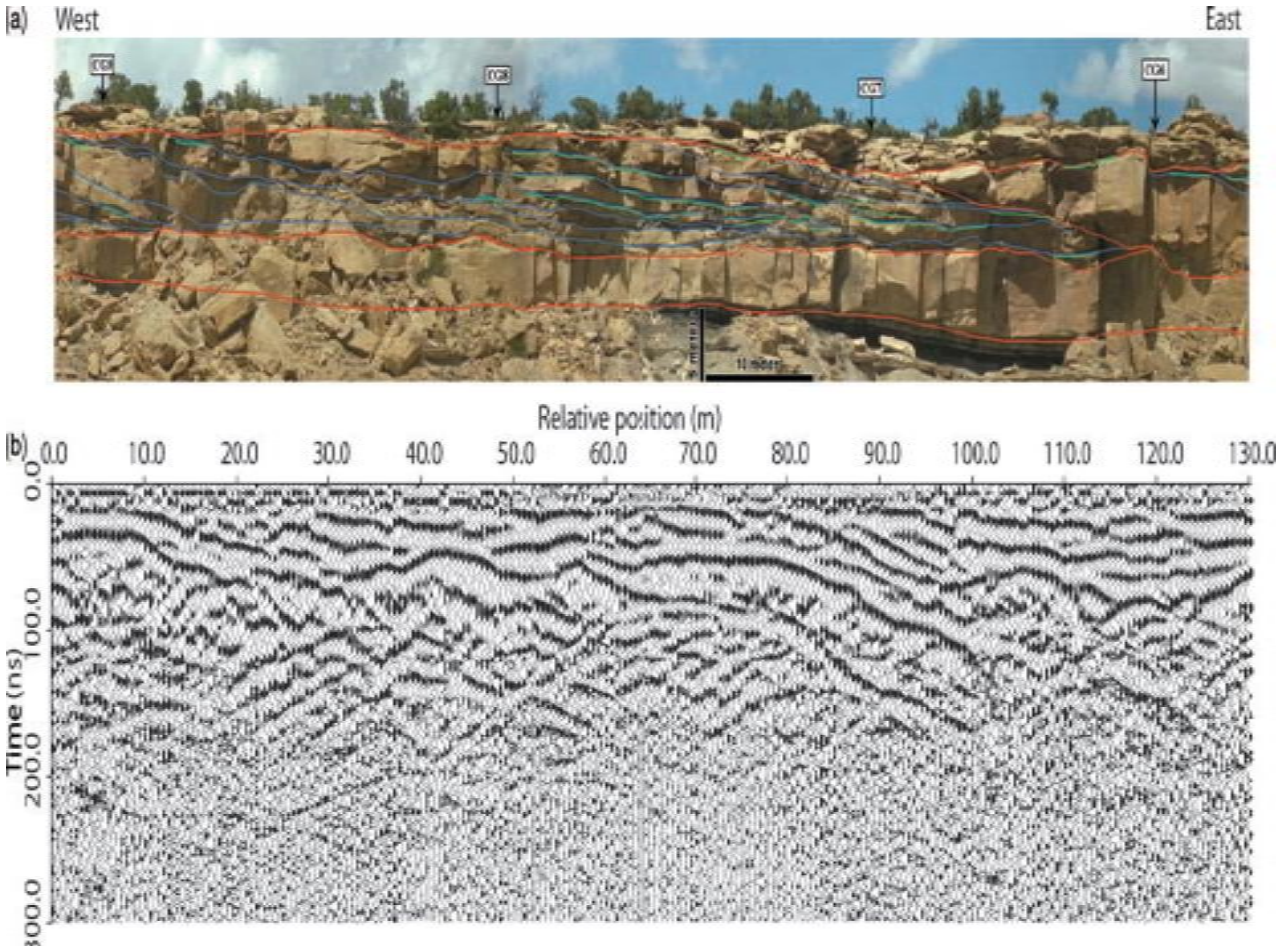

Figure 26: Using outcrop image (a) to interpret GPR section (b) (Zeng, et al., 2004)

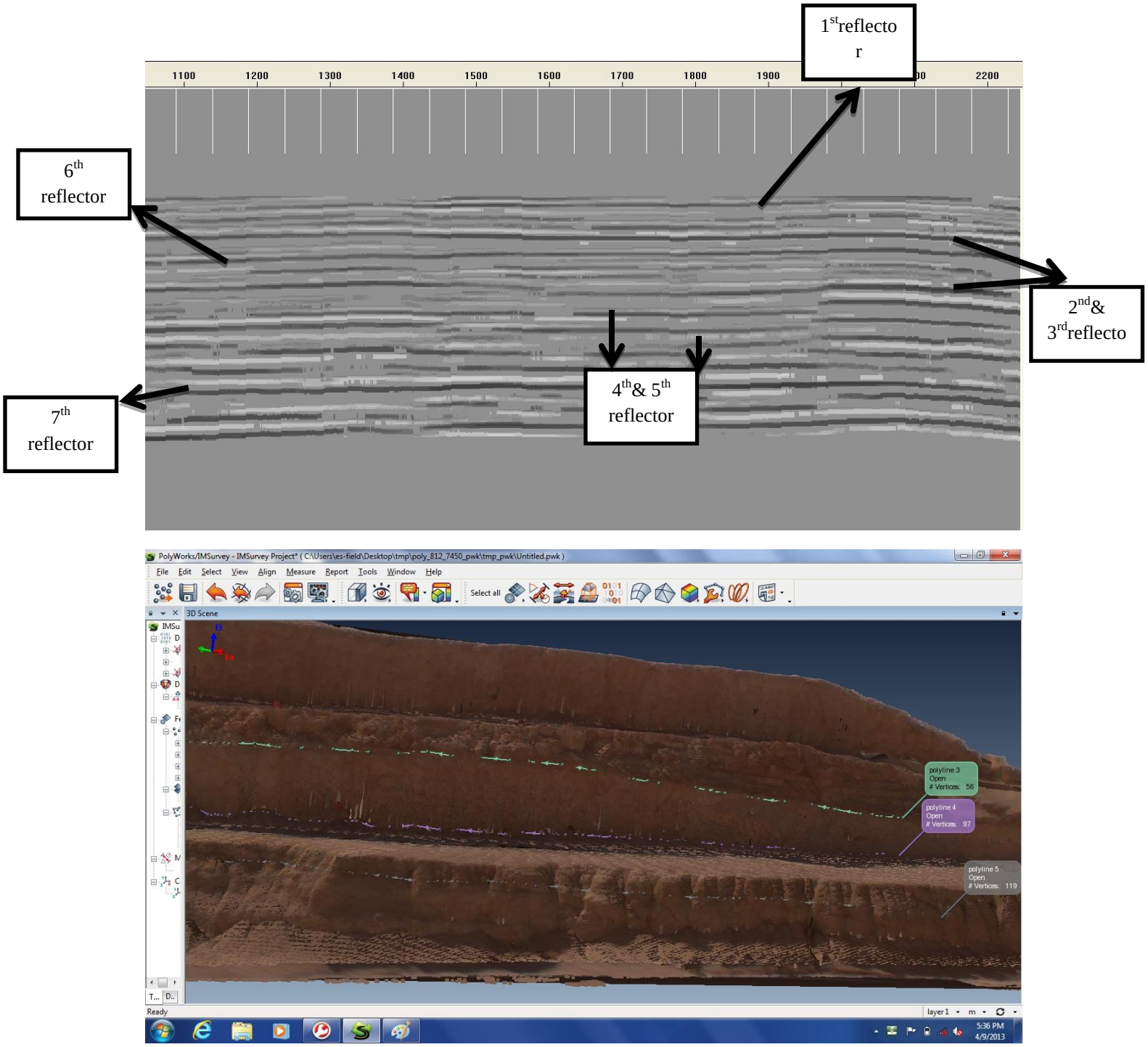

Figure 27: GPR section with seven reflectors (above) and LIDAR point cloud with polylines show the positions of the reflectors (2nd, 3rd, 4th) (bottom)

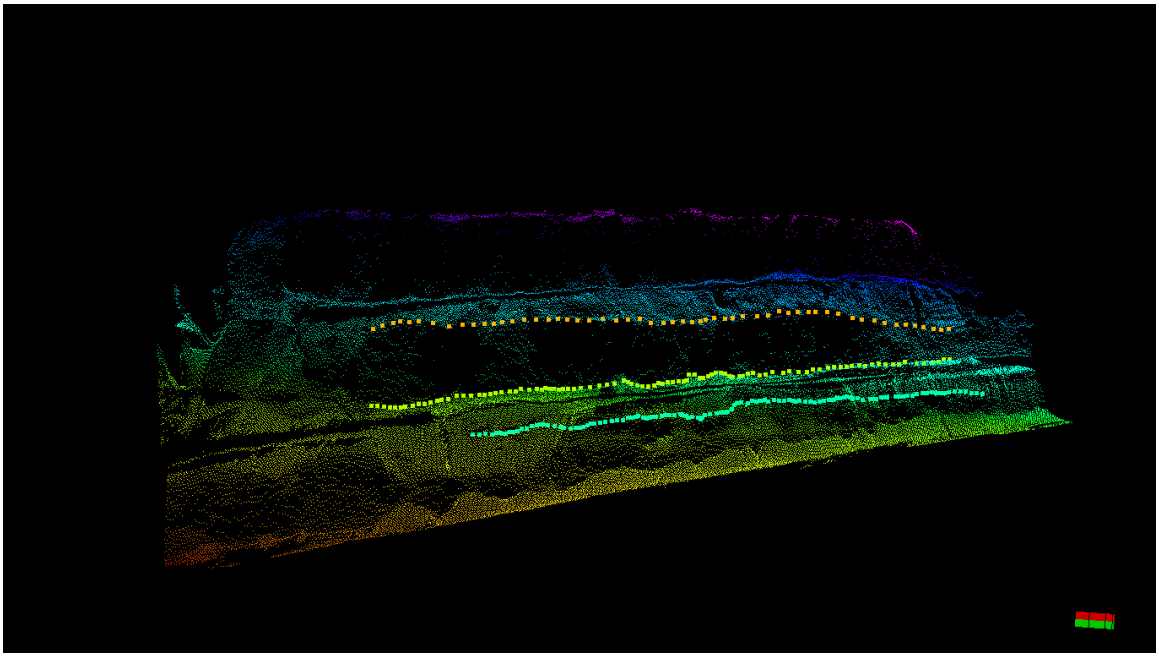

Figure 28: LIDAR mesh point cloud with polylines

Conclusions& Recommendations

Late Miocene Hofuf outcrop in the Shedgumarea shows repetitive fluvial red mudstone and sandstone and fining upward cycles. This part of Hofuf formation shows a fluvial depositional environment and was deposited in meandering stream. The ground penetrating radar succeeded in detecting reflectors within small thickness (13m). Ground penetrating radar succeeded in detecting these reflectors although they are close to each other. This shows that ground penetrating radar is a suitable geophysical method in studying outcrop. Also, GPR proves the cyclicity shown in facies model because the reflectors in the GPR section appeared in some parts and disappeared in others and that due to the change in the mud content. Some of the reflectors detected by GPR could be tracked in LIDAR point cloud. The general porosity of the section is poor because mudstone is dominant.

As recommendation I emphasize thatLIDAR should be used intensively in outcrop studies. After georeferencing the point cloud we can track some outcrop features like boundaries between facies or track the fractures and then determine their directions. Moreover, LIDAR can be integrated with ground penetrating radar because both are high resolution methods as my field study convincingly shows. However, the integration of the two methods should be done in 3D manner. Further integration ofGPR and LIDAR with high resolution sedimentology in 3D will help in characterization the heterogeneity and geometry of reservoir analogs represented in outcrop.

References

Bellian, J. A. ;Kerans, C. ; and Jennette, D.C., "Digital Outcrop Models : Applications Of Terrestrial Scanning Lidar Technology In Stratigraphic Modeling", Journal of Sedimentary Research, vol. 75, No. 2, pp. 166 – 176, March 2005

Falivene, O.; Arbues, P.; Ledo, J.; Benjumea, B.; Munoz, J. A.; Fernandez, O.; and Martinez, S., "Synthetic Seismic Models From Outcrop Derived Reservoir Scale Three Dimensional Facies Models : The Eocene AinsaTurbidite System (Southern Pyrenees)", AAPG Bulletin, vol. 94, No. 3, pp. 317 – 343, March 2010

Franseen,Evan K. ; Byrnes, Alan P. ; Xia, Jianghai; and Miller, Richard D., "Improving Resolution and Understanding Controls on GPR Response in Carbonate Strata: Implications for Attribute Analysis", The Leading Edge, Vol. 26, No. 8, pp. 984-993, Aug 2007

Lee, Keumsuk; Tomasso, Mark; Ambrose, William A.; and Bouroullec, Renaud, "Integration of GPR with stratigraphic and LIDAR data to investigate behind the outcrop 3D geometry of a tidal channel reservoir analog, upper Ferron Sandstone, Utah", The Leading Edge, vol. 26, No. 8, pp. 994-998, August 2007

Lee, Keumsuk; Zeng, Xiaoxian; McMechan, A.; Howell Jr. , Charles D.; Bhattacharya, Janok P.; Marcy, Fanny ; and Olariu, Cornel, "A Ground Penetrating Radar Survey of A Delta Front Reservoir Analog in The Wall Creek Member, Frontier Formation, Wyoming", AAPG Bulletin, vol. 89, No. 9, pp. 1139 – 1155, September 2005

McMechan, George A.; Gaynor, Gerard C.; and Szerbiak, Robert B., "Use of Ground-Penetrating Radar For 3-D Sedimentological Characterization of Clastic Reservoir Analogs", GEOPHYSICS, vol. 62, NO.3, pp. 786 – 796, May – June 1997

Powers, R. W.; Ramirez, L. F.; Redmond, C. D.; and Elberg, E. L., "Geology of the Arabian Peninsula : Sedimentary Geology of Saudi Arabia", US Geological Survey Professional Paper 560-D, pp. 147, 1966

Pringle, J. K.; Howell, J. A.; Hodgetts, D.; Westerman, A. R.; and Hodgson, D. M., "Virtual Outcrop Models of Petroleum Reservoir Analogues: A Review of The Current State of The Art", First Break, vol. 24, pp. 33 – 42, March 2006

Pringle, J. K.; Westerman, A. R.; Clark, J. D.; Drinkwater, N. J.; and Gardiner, A. R., "3D High-Resolution Digital Models of Outcrop Analogue Study Sites To Constrain Reservoir Model Uncertainty : An Example From Alport Castles, Derbyshire, UK", Petroleum Geoscience, vol. 10, pp. 343 – 352, 2004

Pringle, Jamie; Gardiner, Andy; and Westerman, Robin, "Virtual Geological Outcrops – Fieldwork and Analysis Made Less Exhaustive?", Geology Today, vol. 20, No. 2, pp. 67 – 72, March-April 2004

Ruffell, Alastair; Geraghty, Louise; Brown, Colin; and Barton, Kevin, "Ground Penetrating Radar Facies as An Aid to Sequence Stratigraphic Analysis : Application to the Archaeology of Clonmacnoise Castle, Ireland", Archaeological Prospection, 11, pp. 247 – 262, 2004

Saner, Salih; Al-Hinai, Khattab; and Perincek, Dogan, "Surface Expression of the Ghawar Structure, Saudi Arabia", Marine and Petroleum Geology, 22, pp. 657 – 670, 2005

Tomasso, Mark; Bouroullec, Renaud; and Pyles, David R., "The Use of Spectral Recomposition in Tailored Forward Seismic Modeling of Outcrop Analogs", AAPG Bulletin, vol. 94, No. 4, pp. 457 – 474, April 2010

VAN DAM, REMKE L. and SCHLAGER, WOLFGANG, "Identifying causes of ground-penetrating radar reflections using time-domain reflectometry and sedimentological analyses", Sedimentology (2000) 47, 435-449

Van Lanen, Xavier M.; Hodgetts, David; Redfern, Jonathan; and Fabuel-Perez, Ivan, "Applications of Digital Outcrop Models: Two Fluvial Case Studies from The Triassic Wolfville Fm., Canada and Oukaimeden Sandstone Fm., Morrocco", Geological Journal, vol. 44, pp. 742 – 760, 2009

Zeigler, M. A., "Late Permian to Holocene Paleofacies Evolution of the Arabian Plate and its Hydrocarbon Occurrences", GeoArabia, vol. 6, No. 3, pp. 445 – 504, 2001

Zeng, Xiaoxian; McMechan, George A.; Bhattacharya, Janok P. ; Aiken, Carlos L. V.; Xu, Xueming; Hammon III, William S.; and Corbeanu, Rucsandra, "3D Imaging of a Reservoir Analogue in Point Bar Deposits in The Ferron Sandstone, Utah, Using Ground Penetrating Radar", Geophysical Prospecting, vol. 52, pp. 151 – 163, 2004

Vitae

Name	Mohammed Yousef Hussein Abdullah
Nationality	Sudanese
Date of Birth	3/1/1987
Email	jedaih7059@hotmail.com
Academic Background	BSc. of Science in Geophysics